New simulants for martian regolith: Controlling iron variability

Nisha K. Ramkissoon [a,*], Victoria K. Pearson [a], Susanne P. Schwenzer [a], Christian Schröder [b], Thomas Kirnbauer [c], Deborah Wood [b], Robert G.W. Seidel [a], Michael A. Miller [d], Karen Olsson-Francis [a]

[a] STEM Faculty, The Open University, Walton Hall, Milton Keynes, MK7 6AA, UK
[b] Biological and Environmental Sciences, Faculty of Natural Sciences, University of Stirling, Stirling, FK9 4LA, UK
[c] Technische Hochschule Georg Agricola, Herner Straße 45, 44787 Bochum, Germany
[d] Southwest Research Institute, 6220 Culebra Road, San Antonio, TX, 78238, USA

A B S T R A C T

Existing martian simulants are predominantly based on the chemistry of the average 'global' martian regolith as defined by data on chemical and mineralogical variability detected by orbiting spacecraft, surface rovers and landers. We have therefore developed new martian simulants based on the known composition of regolith from four different martian surface environments: an early basaltic terrain, a sulfur-rich regolith, a haematite-rich regolith and a contemporary Mars regolith. Simulants have been developed so that the Fe^{2+}/Fe^{3+} ratios can be adjusted, if necessary, leading to the development of four standard simulants and four Fe-modified simulants. Characterisation of the simulants confirm that all but two (both sulfur-rich) are within 5 wt% of the martian chemistries that they were based on and, unlike previous simulants, they have Fe^{2+}/Fe^{3+} ratios comparable to those found on Mars. Here we outline the design, production and characterisation of these new martian regolith simulants. These are to be used initially in experiments to study the potential habitability of martian environments in which Fe may be a key energy source.

1. Introduction

Geochemical analyses of the martian regolith by instruments aboard the Viking missions showed it to be rich in Fe when compared to terrestrial material (Toulmin et al., 1977). Since then, orbiting spacecraft, exploration rovers and landers, and analyses of martian meteorites have revealed that the martian crust is dominated by rocks of basaltic composition (Edwards et al., 2017; Ehlmann and Edwards, 2014; Filiberto, 2017; McSween et al., 2009; Schmidt et al., 2014) but with chemical variability including silica-rich compositions (e.g., Morris et al., 2016). In addition, deposits rich in sulfates, phyllosilicates and haematite have been identified across the planet's surface indicative of surface processing (Bibring et al., 2005; Bristow et al., 2018; Carter et al., 2015, 2013; Christensen et al., 2000; Cino et al., 2017; Dehouck et al., 2016; Ehlmann and Edwards, 2014; Fraeman et al., 2013; Geissler et al., 1993; Klingelhöfer et al., 2004; Martín-Torres et al., 2015; Morris et al., 2008; Murchie et al., 2009; Mustard et al., 2008; Nachon et al., 2014; Poulet et al., 2007; Squyres et al., 2012; Vaniman et al., 2014; Wray et al., 2009; Yen et al., 2008).

Understanding the complex relationship between 'basaltic' rock compositions and such alteration mineralogy is especially important for interpreting data from missions to Mars, such as Mars 2020 and the ExoMars rover. In addition, missions to Mars also have astrobiological goals, including establishing the potential habitability of key martian environments.

Previous laboratory-based experiments have demonstrated that microorganisms can sequester bio-essential elements from terrestrial basaltic rocks or minerals (Chastain and Kral, 2010; Olsson-Francis et al., 2017; Uroz et al., 2009; Wu et al., 2007) and energy can be obtained from redox reactions centred on H, CO_2, Fe and S (Bauermeister et al., 2014; Kral et al., 2004; Schirmack et al., 2015). Unfortunately, the surface conditions on present-day Mars, and through most of its history, are considered inhospitable. However, terrestrial sites, such as the highly acidic and iron-rich Río Tinto in southwestern Spain (Amils and Fernández-Remolar, 2014) and the highly acidic and hyper-saline Danakil Depression of Ethiopia (Carrizo et al., 2018; Moors and De Craen, 2018), demonstrate that microbial life is capable of growing in extreme environments on Earth. Further, the numerous occurrences of

smectitic clays and other minerals on Mars, characteristic of circum-neutral environments, show that the martian subsurface – and potentially the surface during its earliest history – supported less extreme environments (e.g., Bishop and Rampe, 2016; Bridges and Schwenzer, 2012; Carr and Head, 2010; Ehlmann and Edwards, 2014; Grotzinger et al., 2014; Schwenzer et al., 2016; Squyres et al., 2012).

To test the capabilities of the diverse environments on past or present-day Mars to support life requires controlled laboratory simulation experiments. Thus, it is imperative that geological simulants exist with a realistic diversity of chemical and mineralogical compositions, and that take into account the more detailed chemical conditions that control a microbial habitat: redox and acidity. This paper presents new simulants that represent this diversity.

As will be detailed, the chemical compositions are based on the most recent data regarding the martian surface geology and mineralogy obtained from *in situ* and remote sensing analyses. Importantly, Mars has Fe concentrations greater than that of many terrestrial deposits and, although the planet's distinctive red colour suggests that Fe found on the surface is oxidised (Fe^{3+}), a significant fraction of over 50% of total Fe is found in the form of Fe^{2+} (Klingelhöfer et al., 2004; Morris et al., 2004, 2006a; 2006b; 2008). This paper reports the first simulants to take this factor into consideration.

2. Previous martian analogues and simulants

Materials used for laboratory simulations can generally be divided into two categories: naturally available, terrestrial lithologies (here referred to as 'analogues') and mixtures of natural or artificial materials (here referred to as 'simulants'). The materials detailed in this publication fall into the latter category.

Several terrestrial lithologies have been used as analogues for the martian regolith, for example, the Columbia River Basalts (CRB; Baker et al., 2000) and Salten Skov I (Nørnberg et al., 2009, 2004), and there are rock and mineral stores that comprise of well characterised rocks and minerals to be used as planetary analogues (e.g., the International Space Analogue Rockstore (ISAR; Bost et al., 2013), the Canadian Space Agency's planetary analogue materials suite (Cloutis et al., 2015) and the European Space Agency Sample Analogue Collection (Smith et al., 2018a, 2018b).

There is also a wide range of simulants described in the literature (Table 1). Engineering simulants have been developed and used to replicate the mechanical and physical properties of the martian regolith in order to test hardware and rover mobility (Brunskill et al., 2011; Scott and Saaj, 2009). However, to allow fundamental scientific investigations, including those into habitability, simulants are required that replicate the chemical and mineralogical properties of the martian environment; terrestrial analogues cannot offer this explicit chemical equivalence with Mars.

The concept of a chemical simulant – a rock or mixture of chemically-relevant rock and mineral components - for martian environments is not new. JSC Mars-1(A), the first martian regolith simulant developed (Allen et al., 1998a, 1998b), was made using basaltic ash collected from Pu'u Nene cinder cone, between Mauna Loa and Mauna Kea volcanoes, and has been extensively used in investigations to explore the habitability and the chemical and physical properties of the martian regolith (e.g., Chastain and Kral, 2010; Garry et al., 2006; Gross et al., 2001; Moroz et al., 2009; Phebus et al., 2011). However, this material is highly weathered, with hygroscopic properties that could jeopardise the reproducibility and validity of experimental results. This has led to the development of additional simulants, including Jining Mars Soil Simulant (JMSS-1; Zeng et al., 2015), the Mojave Mars Simulant (MMS; Peters et al., 2008), phyllosilicatic- and sulfatic-Mars Regolith Analogues (P-MRA and S-MRA, respectively; Böttger et al., 2012), Y-Mars (Stevens et al., 2018), MGS-1 (Cannon et al., 2019) and simulants designed by Schuerger et al. (2012) and Fackrell (2018).

JSC Mars-1(A), JMSS-1, MGS-1 and MMS were designed to be representative of a global martian regolith chemistry, but P- and S-MRA were the first simulants designed with the chemical variability of martian regolith in mind. These were intended to be representative of two distinct chemical environments that may have existed on Mars, as determined by orbiter and lander missions at the time they were produced (Böttger et al., 2012): a pH neutral environment and an acidic environment. P- and S-MRA simulants have been widely used in a number of microbiological experiments (Bauermeister et al., 2014; Schirmack et al., 2015), and experiments onboard the International Space Station (Baqué et al., 2016; Pacelli et al., 2017), but their chemistry and mineralogy is generalised.

Other simulants have replicated specific environments on Mars, based on spacecraft data, for example Y-Mars and MGS-1. Y-Mars (Stevens et al., 2018) was designed to replicate the Sheepbed mudstone deposits at Gale Crater, using X-ray diffraction data from CheMin onboard MSL's Curiosity rover to create a mineralogical equivalent; however, its chemical equivalence to the Sheepbed mudstone and Fe^{2+}/Fe^{3+} ratio are unclear. MGS-1 (Cannon et al., 2019) was designed to replicate the Rocknest deposit, at Gale Crater, considered to represent a global basaltic simulant. This took into account the chemistries of both the crystalline and amorphous phases identified within the Rocknest sample by Curiosity and has mineralogical, spectral and physical properties that are similar – but not identical – to the sample on which it was based; there is a 8 wt% discrepancy in MgO and, again, the Fe^{2+}/Fe^{3+} ratio has not been reported.

More recently, Fackrell (2018) proposed designing simulants using combined data from Curiosity, Mars Reconnaissance Orbiter and Mars Global Surveyor. Some of these simulants are comparable with those presented in this paper and also offer different, additional chemistries, but again the Fe^{2+}/Fe^{3+} ratio is not taken into consideration.

Despite the number of simulants that have been developed, there is an increasing need to have chemically-specific simulants for use in experimental procedures, particularly those that have Fe^{2+}/Fe^{3+} ratios representative of that found on Mars. Further, previous simulants have been developed in relatively small quantities to meet only the needs of specific research projects, inhibiting direct comparisons with subsequent studies. Therefore, this paper presents chemically-specific simulants that have been developed in large quantities, and that have been well-characterised, to enable them to be used beyond their original intent.

3. Target martian chemistries

The martian geological record is highly diverse, starting with primary magmatic evolution, continuing with alteration conditions spanning temperatures from boiling in hydrothermal systems to just above freezing in diagenetic subsurface sequences, and to the Noachian–Hesperian climate change that led to desiccation and potentially acidification. Therefore, simulants were designed to replicate the chemistries of four selected environments that were prevalent through Mars' history, as seen from frequent occurrences in a variety of locations on Mars.

3.1. Early basaltic terrain (EB)

Much of Mars is dominated by basaltic material – as original magmatic rocks or broken down into sedimentary materials of basaltic composition (e.g., Glotch et al., 2010; Hamilton et al., 2010; Mustard et al., 2005; Yen et al., 2005). Most of it is significantly different from the regolith analysed by missions to date (Blake et al., 2013; Gellert et al., 2013). In the absence of direct analysis, we have chosen the composition of martian meteorites, specifically the shergottites (Bridges and Warren, 2006), to represent this type of terrain. Shergottites are the youngest and least altered group of martian meteorites, and therefore more representative of basalts found on early Mars. When compared to the general martian regolith composition (Blake et al., 2013; Gellert et al., 2013), basaltic shergottites are richer in Mg, Si and Ca and are compositionally

Table 1
Summary of existing martian regolith simulants and analogues that have been developed (simulants that have only been designed and not yet produced have been omitted).

Simulant/analogue	Developed for	Target environment/ composition	Mineralogy[a]	Material location	Notes
JSC Mars-1(a) (Allen et al., 1998a, 1998b)	Scientific, engineering and education purposes.	Generic martian composition based on spectral data of the Olympus-Amazonis bright region taken by Phobos-2.	*JSC Mars-1:* A mixture of finely crystalline/glassy ash and altered ash particles with Ca-feldspar, some magnetite. Crystalline grains of feldspar, Ti-magnetite, some olivine (Fa_{65}), augite and glass. *JSC Mars-1a:* Volcanic ash. Plagioclase feldspar and minor magnetite. Traces of hematite, olivine, pyroxene and/or glass.	*JSC Mars-1:* Collected from the Pu'u Nene cinder cone, between Mauna Loa and Mauna Kea volcanoes, Hawaii. *JSC Mars-1a:* Tephra mined from the Pu'u Nene cinder cone, Hawaii	• First martian simulants developed. • Developed in large quantities.
Columbia River Basalt (Baker et al., 2000)	Scientific investigations.	Based on martian meteorite chemistries.	Glassy with phenocrysts of sodic anorthite, Fe-rich olivine, and titanomagnetite. Some ilmenite and augite.	Saddle Mountain Series, Columbia River, Oregon, USA.	• A single basalt with a high Fe content (17.6 wt%). • The closest chemistry to global martian regolith (Table 3).
Salten Skov I (Nørnberg et al., 2009, 2004)	Scientific investigations.	Martian drift (dust). Target characteristics determined from Viking, Pathfinder and MER missions.	Natural chemical precipitates of Fe-oxides. Predominantly goethite, hematite and maghemite.	Central Jutland area, Denmark.	• 60 wt% Fe_2O_3.
MMS (Peters et al., 2008)	Specific experiments examining sublimation of water and permafrost.	Global regolith based on data from Viking landers, Pathfinder and MER rovers.	Fine grained texture with scattered phenocrysts of plagioclase. Ca-Rich pyroxene and minor magnetite. Trace amounts of ilmenite, olivine (Fe-rich) and haematite. Some secondary minerals as carbonate and silica. Perhaps barite and apatite. No phyllosilicates or crystalline clays.	Saddleback Basalt (basalt flows interbedded with sediments) near Boron, California, Western Mojave desert.	• Large quantities available. • Available as sand or dust.
SSC-1 and 2 (Scott and Saaj, 2009, 2012)	Hardware testing - microrover trafficability.	No specific site or data reported.	*SSC-1:* a medium grained quartz sand (1.3 mm to <63 μm), containing some silt. *SSC-2:* a fine grained garnet sand (90 μm to < 45 μm).	GMA Garnet group.	• SSC-1 was unwashed, resulting in the inclusion of silt particles.
ES-1,-2 and -3 (Brunskill et al., 2011)	Hardware testing for the ExoMars rover.	Fine dust, fine aeolian sand and coarse sand.	*ES-1:* powdered nepheline (<30 μm) *ES-2 and ES-3:* quartz sand (250–60 and 800-300 μm, respectively).	*ES-1:* Based on Nepheline Stjernoy 7 *ES-2:* Red Hill 110 *ES-3:* Leighton Buzzard DA 30. Material was purchased locally.	• Processing of ES-2 from initial material was not suitable for mass production.
P- and S-MRA (Böttger et al., 2012)	Scientific investigations.	Not based on a specific location. Designed to represent a pH neutral environment and an acidic environment.	Made using various proportions of gabbro, olivine, quartz, haematite, montmorillonite, chamosite, kaolinite, siderite, hydromagnesite, goethite and gypsum.	The Museum fur Naturkunde Berlin and Dr. F. Krantz, Rheinisches Mineralien-Kontor GmbH & Co. KG.	• Represent different chemistries. • Made from a mixture of rocks and minerals.
Simulants developed by Schuerger et al. (2012)	Scientific investigations.	Each simulant was based on one of the following chemistries that have been encountered: basalt, acidic, alkaline, aeolian, Phoenix lander (acidic and perchlorate), and salt.	Made using various proportions of: anhydrite, basalt, calcium carbonate, brushite, ferricopiapite, ferrihydrite, gypsum, halite, haematite, kieserite, jarosite, magnesium chloride, Ti-magnetite, magnesite, olivine, pyroxene, sodium carbonate, sodium perchlorate and sodium sulfate.	Various	• Includes a simulant with perchlorates. • Simulant produced rich in salt.
JMSS-1 (Zeng et al., 2015)	Scientific and engineering purposes.	Global regolith based on Viking landers, Pathfinder, MER rovers and Curiosity.	Jining basalt (93 wt%) - plagioclase, pyroxene, olivine and minor ilmenite Additional hematite (2 wt%) and magnetite (5 wt%) added to increase the Fe content.	Jining basalt, Jining, Inner Mongolia, northern edge of the North China Craton. Magnetite and haematite from the Hebei province in China.	• A mixture of basalt and minerals to produce chemistry similar to the required martian chemistry.
	Engineering purposes	Range of rocks that can be combined to represent	Rocks with orthoclase, plagioclase pyroxene, olivine	Banks Peninsula area, South Island, New Zealand.	• Custom or target Mars simulants can be made.

(continued on next page)

Table 1 (*continued*)

Simulant/analogue	Developed for	Target environment/ composition	Mineralogy[a]	Material location	Notes
Banks Peninsula Rocks (Scott et al., 2017)	(construction and developing of infrastructure on Mars).	specific chemistries, e.g., Gusev crater.	and magnetite. Not all rocks contain olivine, but all possess <10 wt% magnetite.		• Could be produced in large quantities.
Y-Mars (Stevens et al., 2018)	Scientific investigations	Curiosity data from Sheepbed Formation, Gale crater.	A mixture of: albite, saponite, augite, magnetite, enstatite, dunite, anhydrite, sanidine, pyrrhotite, selenite.	Various environmental sources.	• Simulant of a martian sedimentary environment. • Based on mineralogy. • Simulant pressed into pellets to represent burial.
MGS-1 (Cannon et al., 2019)	Scientific investigations	Representative of a global basaltic chemistry based on Rocknest in Gale crater, using data from Curiosity.	Made from a mixture of: plagioclase, pyroxene, olivine, magnetite, haematite, anhydrite, quartz, ilmenite, basaltic glass, opal, Mg-sulfate, ferrihydrite and Fe-carbonate.	Commercially available materials used where possible, e.g., Mg-sulfate purchased as Epsom salt, Fe-carbonate purchased as ferrous carbonate and magnetite purchased as black iron oxide.	• Currently only prototype produced. • Attempted to reproduce the chemistry of both crystalline and amorphous phases.
International Space Analogue Rock store (Bost et al., 2013)	Instrument testing.	Representative of different martian environments.	A range of volcanic, magmatic, sediments and clays.	Various.	• Characterised using optical microscopy, XRD, Raman spectroscopy, IR spectroscopy, Mössbauer spectroscopy, EDS, EMPA, ICP-AES and ICP-MS.
CSA Planetary analogue suite (Cloutis et al., 2015)	Scientific experiments and instrument testing.	Representative of various chemistries and based on different martian environments	Various	Various.	• Characterised using EMPA, optical microscopy, Raman spectroscopy, XRF, laser induced fluorescence spectroscopy, reflectance spectroscopy and thermal infrared emission spectroscopy.
European Space Agency Sample Analogue Collection (ESA[2]C; Smith et al., 2018a, 2018b, 2017)	Engineering and science payload development.	Basalt, clay granules (sepiolite and attapulgite) and clay powders (a range of bentonite).	Various	Various	• Chemical properties determined *via* ICP-AES, ICP-MS, SEM, EMPA and XRD analysis. • Grain size, grain shape, bulk density, bulk porosity, shear strength, compressive strength and tensile strength determined.

[a] Chemical data for scientific simulants are presented in Table 3.

similar (with the exception of Al and Fe compositions) to an 'average' terrestrial basalt (Table 2). The chemical composition of the Zagami shergottite meteorite, which was considered representative of the basaltic shergottites (Bridges and Warren, 2006; Ding et al., 2015), was used to indicate the composition required from the "early basaltic" simulant (Table 2).

3.2. Sulfur-rich regolith (SR)

The overall composition of martian regolith is one of general enrichment in S (as sulfur and sulfates; Franz et al., 2019) when compared to terrestrial basalts (Table 2). Martian regolith enriched with sulfates are referred to as "Paso Robles class soils" (after the site at which they were first detected), with S found in the form of Mg-, Ca- and Fe-sulfates (Lane et al., 2008; Yen et al., 2008). The exact formation mechanism for the Paso Robles regolith is still unclear, but is has been suggested to have formed as a result of magma degassing causing fumarolic or hydrothermal condensates to deposit (Yen et al., 2008).

The Paso Robles regolith was detected and analysed by the Alpha Particle X-ray Spectrometer (APXS) aboard Mars Exploration Rover Spirit at Columbia Hills and has one of the highest S concentrations identified on Mars to date (Gellert, 2013b; Gellert et al., 2006). The Paso Robles composition used as the basis for the sulfur-rich simulant is shown in Table 2.

3.3. Haematite-rich regolith (HR)

Haematite is widespread across the martian surface. It is believed that haematite most likely formed in oxidising, potentially aqueous, environments. It has also been suggested that the formation was the result of thermal oxidation of volcanic ash (Hynek, 2002). A large deposit of crystalline haematite was identified in Sinus Meridiani by the Thermal Emission Spectrometer (TES) aboard Mars Global Surveyor (Christensen et al., 2000), Curiosity has observed haematite enrichments at Gale crater, and the Mars Reconnaissance Orbiter has identified deposits at Candor Chasma (Fergason et al., 2014; Fraeman et al., 2013; Geissler et al., 1993; Weitz et al., 2008).

The landing site of the Mars Exploration Rover Opportunity at Meridiani Planum was selected to investigate the source of the Sinus Meridiani haematite. This indicated that millimetre-sized haematite-rich spherules weather out from the S-rich Burns formation, which underlies much of Meridiani Planum. These form a lag deposit on top of a basaltic soil unit that covers the area (Klingelhöfer et al., 2004; Soderblom et al., 2004). Chemical analysis of regolith at Hematite Slope at Meridiani Planum, carried out by Opportunity's APXS, determined a high total Fe content of 26.5 wt% for a sample known as Hema2 (Rieder et al., 2004), attributed to the presence of haematite spherules (Calvin et al., 2008).

The chemistry of the haematite-rich simulant presented here is based on the composition of the Hema2 sample (Rieder et al., 2004) (Table 2)

Table 2
Chemical compositions of the four target martian chemistries. Data on the Zagami meteorite was used for the shergottite chemistry.

Oxide	General terrestrial basalt[a]	Shergottite[b]	Paso Robles[c]	Hematite Slope[d]	Rocknest[e]
Na_2O	2.76	1.23	1.60	1.50	2.53
MgO	6.01	11.30	5.53	7.00	5.24
Al_2O_3	18.04	6.05	4.13	8.10	9.68
SiO_2	51.33	50.50	21.80	41.90	44.62
P_2O_5	0.16	0.40	5.61	0.83	0.32
SO_3	–	0.49[g]	31.70	4.68	5.54
Cl	–	–	0.55	0.46	0.92
K_2O	0.82	0.14	0.19	0.43	1.14
CaO	10.07	10.50	6.84	6.27	7.06
TiO_2	1.10	0.79	0.62	0.83	1.41
Cr_2O_3	–	–	0.04	0.37	0.18
MnO	0.16	0.50	0.25	0.32	0.36
FeO[f]	9.10	18.10	21.00	26.50	20.40
Total	99.55	100.00	99.19	99.86	99.60

[a] Nockolds (1954).
[b] Bridges and Warren (2006).
[c] Gellert et al. (2006).
[d] Rieder et al. (2004).
[e] Gellert et al., (2013)
[f] All Fe has been reported as FeO.
[g] Taken from Ding et al. (2015).

because it has one of the highest concentrations of total Fe (Gellert, 2013b; Gellert et al., 2006).

3.4. Contemporary Mars regolith (CM)

Previous martian simulants (e.g., JSC Mars-1(1a), JMSS-1, MGS-1 and MMS (Allen et al., 1998a, 1998b; Cannon et al., 2019; Peters et al., 2008; Zeng et al., 2015) were developed to represent a global Mars regolith composition. Although this is not ideal for investigating specific environments, to enable comparisons between previous simulant studies, an equivalent 'global' simulant was designed and is presented here based on the Rocknest chemistry at Gale Crater (Blake et al., 2013; Gellert et al., 2013). Data obtained by the Viking, Pathfinder and MER missions showed the regolith (with the exception of that enriched by Fe or S) to be very similar in composition across the planet (e.g., Yen et al., 2005), with <3.5 wt% variation in major oxides (except for SiO_2 and total Fe which had variations in chemistry of 5.80 and 6.11 wt %, respectively). These chemistries were averaged to produce a mean "global" chemistry. Rocknest, analysed by the APXS on board the Curiosity rover, has been shown to have an overall chemistry within $<\pm2.5$ wt% of this averaged composition and has therefore been used as the "contemporary Mars" simulant target composition (Table 3).

Table 4 summaries the key characteristics and justification for each of the selected target environments.

4. Simulant specification

4.1. Importance of Fe^{2+}/Fe^{3+} ratio

Martian lithologies have total Fe abundances that are higher than terrestrial basalts (in the range of 12–16 wt% compared to, on average, approximately 3–10 wt%); regolith from Meridiani Planum contains up to 22 wt% total Fe (Rieder et al., 2004). Generally, pre-existing simulants have 2.92–4.20 wt% less total Fe than the average martian regolith, because their major components are, generally, terrestrial rocks. The total Fe content of the CRB analogue is more in line with the martian regolith (17.76 wt %), but the Mg concentration is lower than required and is approximately 3 wt% enriched in Ti and Al compared to the target martian chemistries (Table 3; Baker et al., 2000). Salten Skov I has a total Fe concentration of 60.46 wt% and has been used to represent martian

dust, but this exceeds the target Fe concentration. The total Fe concentration of JMSS-1 was elevated by adding magnetite and haematite (which increased Fe_2O_3 concentration by ~5 wt%; Zeng et al., 2015). However, the total Fe concentration of JMSS-1 was still only 16 wt% (as Fe_2O_3).

Whilst total Fe content can, theoretically, be increased in a new simulant, this does not provide a complete representation of Fe chemistry on Mars; Fe on Mars is estimated to be predominantly (50–90%) in the form of Fe^{2+} (Morris et al., 2004, 2006a; 2008). Not all data obtained from analyses of the regolith has discriminated between Fe^{2+} and Fe^{3+}, but measurements taken by Spirit's Mössbauer spectrometer detected Fe^{2+} concentrations in the regolith of the Gusev plains of between 78 and 59 wt% of total Fe (Morris et al., 2004, 2006a; Wang et al., 2006). Mössbauer analysis of JSC Mars-1 conducted by Moroz et al. (2009) showed that approximately 80% of the Fe was in the form of Fe^{3+}, which is greater than the concentration expected on Mars. Crucially, since variations in the Fe^{2+}/Fe^{3+} ratio is important for microbial metabolism - for example, Fe^{2+} can be oxidised by terrestrial microorganisms to produce energy - the Fe^{2+}/Fe^{3+} ratio is an important factor when exploring martian habitability (Nixon et al., 2013; Schröder et al., 2016). Therefore, it is important to represent variations in the Fe^{2+}/Fe^{3+} ratio within a simulant. However, none of the pre-existing simulants have taken this into consideration or have been provided with data on this ratio.

Given this requirement, the simulants were designed to contain 50-90 wt% of total Fe as Fe^{2+}, facilitated in such a way to enable the Fe^{2+}/Fe^{3+} ratio to be varied at a future date depending on experimental requirements or if future missions revealed further compositional variations. Additionally, the overall chemistry of the simulants was designed to match (within 5%) the respective martian target chemistries (Table 3); this similarity was only previously achieved with the CRB analogue, although its Fe^{2+} concentrations were not reported.

4.2. Practical considerations

The specification of the simulants considered the chemical and mineralogical factors discussed above, but other factors were important. For example, the components needed to be readily sourced, available in large quantities (50 kg was estimated for each simulant), and the total cost needed to be kept within budgetary constraints. To ensure reproducibility of subsamples of the simulants, the constituents also needed to be chemically homogenous.

A mixture of rocks and minerals was proposed, which permitted control over the concentrations of major rock forming elements and the Fe^{2+}/Fe^{3+} ratio; this would not be possible with a single rock sample (e.g., basalt). This enabled the simulants to also contain the same minerals as those likely to be found on Mars, where possible (McSween et al., 2009, 2004; Ehlmann and Edwards, 2014) (Table 5). In reality, ideal minerals were substituted by minerals or rocks with a similar chemistry when availability or cost was a barrier.

While the simulants were not designed to replicate the physical properties of the martian regolith they could be reproduced cost-effectively to different physical specifications. Some physical properties of the final simulants have been characterised and are presented in this paper.

4.3. Mineralogical requirements

To match the required chemistries shown in Table 2, an initial review of common terrestrial mineral compositions was undertaken (Deer et al., 1992; Nockolds, 1954) and candidate minerals selected. These were then limited to minerals known to be present on Mars, as identified by McSween et al. (2009, 2004) and Ehlmann and Edwards (2014) (Table 5).

Since large quantities (50 kg) of all simulants were required, to reduce the overall cost, a terrestrial, basaltic rock was considered to be the ideal base component, since it is most similar in lithology to the target martian

Table 3

Martian regolith chemical compositions taken from various lander missions compared with the chemical compositions of pre-existing martian simulants. Values in bold represent chemical differences of ±5 wt% when compared to the martian regolith chemistry. Banks Peninsula was compared to Gusev Crater, S-MRA was compared with Paso Robles and the remaining simulants were compared to average global chemistry.

		Na_2O	MgO	Al_2O_3	SiO_2	P_2O_5	SO_3	Cl	K_2O	CaO	TiO_2	Cr_2O_3	MnO	FeO	Total
Martian chemistries															
Viking 1	landing site, undisturbed fines[a]	–	5.67	7.33	43.30	–	6.57	0.65	0.00	5.93	0.66	–	–	16.62	86.76
	landing site, deep fines[a]	–	6.00	7.25	44.00	–	6.70	0.80	0.04	5.70	0.63	–	–	15.74	86.86
Viking 2	landing site, undisturbed fines[a]	–	–	–	43.00	–	8.00	0.30	0.03	5.88	0.62	–	–	16.73	74.56
	landing site, deep fines[a]	–	–	–	42.00	–	7.75	0.35	0.00	5.50	0.51	–	–	15.56	71.66
Pathfinder	landing site, Ares Vallis[b]	1.09	8.69	7.98	42.30	0.98	6.79	0.55	0.61	6.53	1.01	0.30	0.52	20.06	97.41
	soil next to yogi[c]	3.20	8.00	10.60	41.00	1.20	6.90	0.80	0.50	5.60	1.00	0.40	0.40	18.35	97.95
	next to yogi[c]	3.20	7.10	10.40	40.70	0.60	5.70	0.80	0.50	6.10	0.40	0.50	0.20	21.32	97.52
	disturbed soil next to scooby[c]	2.60	6.40	10.20	41.70	0.80	6.60	1.20	0.70	6.40	0.80	0.20	0.10	19.97	97.67
Spirit	Gusev Crater[d]	3.20	9.10	10.00	46.50	0.93	6.36	0.51	0.45	6.03	0.80	0.29	0.31	15.80	100.28
Opportunity	Meridiani Planum bright soils[e]	2.31	7.62	9.21	45.33	0.91	7.23	0.81	0.50	6.66	0.99	0.34	0.36	17.59	99.86
	Meridiani Planum, Eagle crater[f]	1.40	7.20	8.80	45.50	0.82	4.93	0.43	0.48	7.52	1.09	0.52	0.40	20.10	99.79
MSL	Rocknest Gale crater soil[g]	2.72	8.69	9.43	42.88	0.94	5.45	0.69	0.49	7.28	1.19	0.49	0.41	19.19	99.85
Average of the global chemistry		2.47	7.45	9.12	43.19	0.90	6.58	0.66	0.36	6.26	0.81	0.38	0.34	18.09	94.86
Martian Simulants															
JSC Mars-1[h]		2.40	3.40	**23.30**	43.50	0.90	–	–	0.60	6.20	3.80	–	0.30	14.04	100.00
JSC Mars-1A[i]		2.50	3.50	**23.50**	44.00	0.90	–	–	0.60	6.00	4.00	–	0.30	14.30	100.80
JMSS-1[j]		2.92	6.35	13.64	**49.28**	0.30	–	–	1.02	7.56	1.78	–	0.14	14.40	98.99
MMS[k]		3.28	6.35	**17.10**	**49.40**	0.30	**0.10**	–	0.48	10.45	1.09	0.05	0.17	**9.78**	99.64
Banks Peninsula, e.g., composition for Gusev crater[l]		3.70	7.74	13.36	48.23	0.60	–	–	1.54	9.05	2.55	0.00	0.18	11.21	98.60
Salten Skov I[m]		0.19	**0.16**	3.20	**16.10**	**0.47**	–	–	0.52	**0.20**	0.29	–	1.66	**55.86**	84.71
P-MRA[n]		0.30	4.52	11.90	43.60	0.56	**0.20**	–	1.07	4.74	0.45	–	0.17	18.26	87.81
S-MRA[n]		1.09	**10.90**	**9.20**	**31.80**	0.42	**9.10**	–	0.86	**18.40**	0.98	–	0.41	17.90	103.06
Columbia River basalt[o]		2.43	4.38	12.35	47.09	1.58	–	–	1.39	8.84	3.65	–	0.32	17.65	99.68
MGS-1[p]		3.40	**16.70**	8.90	50.8	0.4	2.1	–	0.30	3.70	0.30	0.10	0.10	13.30	100.0

[a] Clark et al., (1982).
[b] Wänke et al., (2001).
[c] Foley et al., (2003).
[d] Gellert et al., (2004).
[e] Clark et al., (2005).
[f] Rieder et al., (2004).
[g] Blake et al., (2013).
[h] Allen et al., (1998a).
[i] Allen et al. (1998b).
[j] Zeng et al., (2015).
[k] Peters et al., (2008).
[l] Scott et al.,(2017).
[m] Nørnberg et al., (2004).
[n] Böttger et al., (2012).
[o] Baker et al., (2000).
[p] Cannon et al., (2019).

Table 4

Overview of selected target environments.

	EB	SR	HR	CM
Representative target environment	Early and young basaltic terrain.	Sulfur- rich regolith.	Haematite-rich regolith.	Global and contemporary surface regolith.
Target chemistry[a]	Zagami meteorite, shergottite meteorite.	Paso Robles, Columbia Hills.	Hema2 sample, Meridiani Planum.	Rocknest, Gale Crater.
Justification for target selection	Shergottites are the youngest group of martian meteorites, and the Zagami was considered representative of basaltic shegottites.	Possess one of the highest concentrations of sulfur identified for this class of sulfur rich soils.	Possess one of the highest concentrations of total Fe found on Mars.	It is considered representative of a widespread regolith chemistry that has been identified in previous missions.
Possible formation environment	Magmatic activity.	Magmatic fumarole or the condensation of hydrothermal gases.	Oxidising, possibly aqueous.	Aeolian environment.

[a] Target chemistry and known mineralogy of target locations are summarised in Tables 2 and 5

environments. Additional minerals could be added to this to achieve greater chemical specificity. Terrestrial rocks of basaltic compositions also provide a source of pyroxene minerals, one of the primary framework silicates detected in the martian crust (Ehlmann and Edwards, 2014); isolated pyroxenes were difficult to source in sufficient quantities

and so a pyroxene-rich leucite phono-tephrite (referred to as phono-tephrite) was selected (see Section 4.2). The basaltic rock chosen was also olivine-free (Fig. 1), allowing the Mg content to be better controlled by the addition of dunite.

To achieve Fe variability, an Fe-rich blasting sand (referred to as Fe-

Table 5
Target mineralogy of selected sites.

Rocknest[a]	Paso Robles class[b,c]	Haematite Slope[d]	Shergottite[e]
Plagioclase	Ferric iron sulfates	Nanophase ferric oxide	Augite
Olivine	Silica	Pyroxene	Pigeonite
Augite	Mg- sulfates	Olivine	Plagioclase
Pigeonite	Ca-sulfates	Haematite	Hydrous amphibole
Magnetite	Ca-phosphate		Ti-magnetite
Anhydrite	Haematite		Ilmenite
Quartz			Apatite
Sanidine			Pyrrhotite
Haematite			Glass
Ilmenite			
Amorphous phase			

[a] Bish et al. (2014).
[b] Lane et al. (2008).
[c] Yen et al. (2008).
[d] Klingelhöfer et al. (2004).
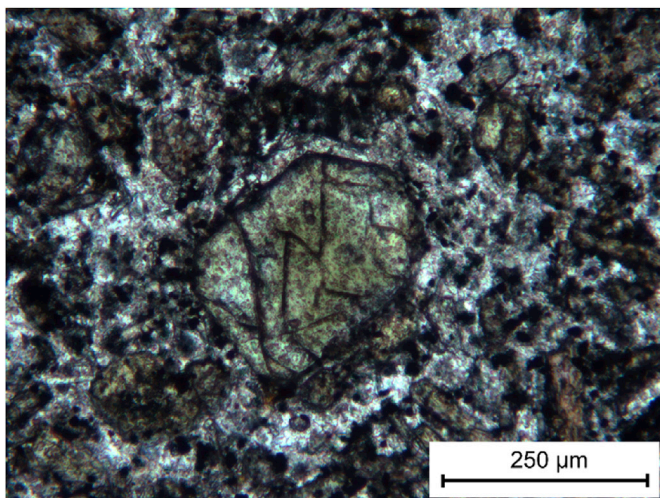[e] Bridges and Warren (2006).

Fig. 1. Phono-tephrite, used as the basaltic base component. The image shows a phenocryst of pyroxene within a micro-crystalline to fine-grained matrix of feldspar and feldspathoids. Image taken using a transmission light microscope in plane polarised light.

silicate glass) was used as a distinct source of Fe, rich in Fe^{2+} (Schwenzer et al., 2017). Ideally, a fayalite would be used as a source of Fe^{2+}, however it was not available in the quantities required; the Fe-silicate glass has a similar chemistry to fayalite, and so was considered a suitable substitute.

The use of a separate source of Fe^{2+} allowed for modification of the Fe^{2+}/Fe^{3+} ratio, and this could be balanced using haematite and quartz, since the Fe-silicate glass was also rich in Si. Therefore, it was possible to modify the contemporary Mars and early basaltic Mars simulants to have Fe^{2+} concentrations of 50 wt% of total Fe as Fe^{2+}, and the haematite-rich simulant to have 90 wt% of total Fe as Fe^{2+}. This allowed a suite of simulants to be developed that covered the range of total Fe^{2+} concentrations shown to exist on Mars (Klingelhöfer et al., 2004; Morris et al., 2004, 2006a, 2006b, 2008, Tables 6 and 7).

Some compromises were needed where availability or cost precluded the use of the most relevant minerals. For example, albite (Na-rich plagioclase feldspar) and anorthite (Ca-rich plagioclase feldspar) were identified as required minerals, but it was not possible to obtain either of these in sufficient quantities. Instead, anorthosite (an intrusive igneous rock that is approximately 90% plagioclase feldspar) was used as a

Table 6
Proportion (in wt%) of each material used to produce standard simulants.

	OUEB-1	OUSR-1	OUHR-1	OUCM-1
Fe-silicate	30	10	19	30
Phono-tephrite	10	27	27	40
Quartz	14	0	3	3
Dunite	19	8	11	8
Anorthosite	12	0	6	7
Wollastonite	12	0	3	3
Pyrite	0	40	6	4
Magnetite	2	3	4	3
Apatite	1	7	1	1
Gypsum	0	5	0	1
Haematite	0	0	20	0

Table 7
Proportion of each component used to make simulants with modified Fe^{2+} concentrations.

	OUEB- 2	OUSR- 2	OUHR- 2	OUCM- 2
Fe-silicate	14	0	39	11
Phono-tephrite	10	27	27	40
Quartz	16	5	2	8
Dunite	19	8	11	8
Anorthosite	12	0	6	7
Wollastonite	12	0	3	3
Pyrite	0	40	6	4
Magnetite	2	0	4	3
Apatite	1	7	1	1
Gypsum	0	5	0	1
Haematite	14	8	1	14

substitute for both types of feldspar, because its Ca:Na ratio is similar to the martian chemistries required (Table 2).

One of the most significant compromises was the substitution of Fe-sulfates for Fe-sulfides. Paso Robles class soils on Mars (OUSR-1 target composition) are dominated by Fe-sulfates (Lane et al., 2008; Morris et al., 2008; Yen et al., 2008), however the lack of availability of Fe-sulfates at the quantities required meant an alternative was needed that would balance both the Fe and S content. Pyrite was therefore selected.

5. Simulant production

5.1. Sourcing simulant components

The phono-tephrite was collected from a Quaternary lava flow near Mayen in the Eifel region, Germany. The 100 000 to 150 000 year old lava flow originates from the Bellerberg volcano near Ettringen, and is 15–20 m thick at its centre (Van den Bogaard and Schmincke, 1990). The lava flow has previously been mined because of its suitability for making mill stones. Today it is mined by MAYKO Natursteinwerke GmbH & Cie. KG, who facilitated the collection of sample materials (Fig. 2).

Additional materials were obtained from Northern Geological Supplies Ltd. (dunite, quartz, gypsum, magnetite, pyrite, anorthosite and haematite), Dr. F. Krantz, Rheinisches Mineralien-Kontor GmbH & Co. KG (apatite) and SIBELCO (wollastonite). The Fe-silicate glass is a by-product of copper smelting and was obtained from Scangrit, UK. Test samples were provided by the various suppliers, in order to: confirm their composition and homogeneity, identify any inclusions that should be avoided, and confirm suitability for use before larger quantities were ordered and a full characterisation completed.

5.2. Test samples

Test materials were obtained from appropriate suppliers as hand specimens (between 3 and 10 cm in length for the phono-tephrite, haematite and apatite, anorthorsite, quartz, dunite, pyrite, magnetite

Fig. 2. Columns of the Mayen lava flow, taken from the quarry from which the phono-tephrite was collected (Germany).

and gypsum) or as crushed particles <4 mm and <2 mm (Fe-silicate glass and wollastonite, respectively), and prepared for characterisation.

Large specimens were cut using a diamond saw into 1–2 cm diameter subsamples, and representative subsamples of the Fe-silicate glass and wollastonite were taken. Each were embedded into epoxy resin and polished for characterisation *via* scanning electron microscopy-energy dispersive spectroscopy (SEM-EDS), electron microprobe analysis (EMPA) and Raman spectroscopy, which confirmed the mineralogy and chemistry of the specimens. Based on this data, the proportions of each component could be adjusted to ensure the correct elemental compositions were achieved for the final simulants, and to identify compositional heterogeneities.

5.3. Simulant preparation

Once the bulk chemistry had been refined according to the results from the test samples, larger quantities of the component materials were purchased. Preparation of the simulants were conducted using the crushing facility at The Open University, UK. Large specimens (>4 cm) of phono-tephrite, anorthosite, quartz, dunite, pyrite, magnetite, haematite and gypsum were split into smaller pieces using a rock splitter. The jaw crusher crushed rock specimens (~4 cm) into particles <0.5 mm–3mm in size, which were then sieved into the following fractions: >900 μm, 900–400 μm, 400-300 μm, 300–280 μm and <280 μm. Wollastonite and Fe-silicate grains were supplied crushed as grains, which were <4 mm and <2 mm, respectively, meaning only sieving was required.

The five particle size fractions generated for each simulant (>900 μm, 900–400 μm, 400-300 μm, 300–280 μm and <280 μm) are within the ranges identified for regolith on Mars. For example, Shorthill et al. (1976), using Viking I data, identified particles 10–2000 μm for material at or near the surface. Weitz et al. (2006), using images taken at Meridiani Planum by the Opportunity rover, found two distinct populations of grain sizes, one <125 μm and the other between 1 and 4.5 mm (with the latter dominated by haematite concretions). Cabrol et al. (2008) analysed images of particles along Spirit's transverse, also showing two dominant particle size ranges of 420–105 μm and 1630-840 μm, however the mean particle sizes were 960–260 μm. A more recent study by Weitz et al. (2018) examined particles size at Gale Crater, again identifying two dominant size ranges: 250–50 and 500-300 μm. On the basis of these studies, the particle size fractions selected for these simulants are within the range found on Mars.

Since the 900–400 μm fraction was to be used in initial experiments, this fraction was washed to remove fine grained particulates that may have adhered to the crystal surfaces. The components were washed three times in acetone for 5 min in an ultrasonic bath, and rinsed twice with deionised water after each wash to dislodge any fine grained particles. To remove the acetone, the process was repeated using deionised water instead of acetone; however, gypsum was washed five times using deionised water. To ensure that fine grained particles were removed, the samples were washed through a sieve and then dried for 24 h, at 65 °C. The washed components were then weighed and mixed together in the proportions detailed in Tables 6 and 7 The mixtures were agitated to achieve homogeneity.

6. Simulant characterisation

6.1. Scanning electron microscopy-energy dispersive spectroscopy (SEM-EDS)

SEM-EDS was conducted to obtain qualitative compositional data on the test samples, specifically to confirm their mineralogy and homogeneity.

The test samples embedded in epoxy blocks were carbon coated and analysed using a dual beam FEI Quanta 3D microscope, equipped with an Oxford Instruments energy dispersive X-ray detector, using a 20 kV gallium ion beam. SEM-EDS maps and backscattered electron images were taken of polished samples to obtain an overview of each of the test samples, and provide a bulk chemistry that was used to finalise the quantities of each material required to make the simulants (Table 8).

6.2. Electron microprobe analysis (EMPA)

EMPA was conducted to obtain quantitative chemical data for the dominant mineral phases in each test sample. EMPA analysis was conducted using a Cameca SX100 microprobe equipped with five spectrometers. All samples were analysed using a 10 μm beam diameter and at 20 kV/20 nA. Quantitative compositions were calculated using the following mineral standards: feldspar (Si, Al and K), jadeite (Na), LiF (F), forsterite (Mg), bustamite (Mn and Ca), willemite (Zn), sylvite (Cl), barite (S in silicate and sulfates), haematite (Fe in oxides and silicates), pyrite (S and Fe in sulphides), rutile (Ti), Cr_2O_3 (Cr), Cu metal (Cu), YPO_4 (P and Y), and zirconia (Zr). The detection limits (in wt%) for each element were

Table 8
Bulk chemistry determined by SEM-EDS analysis.

	Phono-tephrite	Fe-silicate glass	Anorthosite	Quartz	Dunite	Apatite	Pyrite	Magnetite	Gypsum	Haematite	Wollastonite
Na_2O	6.57	1.35	4.64	0.08	–	–	–	–	0.15	–	–
MgO	4.20	1.31	–	–	49.6	–	0.03	2.73	0.09	–	1.12
Al2O3	16.66	4.78	27.49	–	–	–	0.04	1.7	0.03	–	–
SiO_2	51.29	39.14	52.96	98.71	42.8	21.08	0.29	8.18	0.32	34.97	54.02
P_2O_5	–	0.47	–	–	–	32.03	–	–	–	–	–
SO_3	0.53	1.11	–	–	–	1.03	65.09	0.04	56.63	–	–
Cl	0.20	–	0.14	–	0.17	0.15	–	–	–	–	0.71
K_2O	5.56	0.46	0.28	–	–	–	–	0.04	–	–	–
CaO	8.18	3.93	13.62	–	0.04	45.63	0.06	2.59	42.24	–	43.49
TiO_2	1.62	0.29	0.04	–	–	–	–	0.02	–	–	–
Cr_2O_3	0.03	0.34	0.02	–	0.72	–	–	0.03	–	–	–
MnO	0.15	0.54	–	–	0.1	–	–	0.32	0.04	–	–
FeO	5.92	45.91	0.53	0.02	6.44	–	32.86	83.89	–	–	–
Fe_2O_3	–	–	–	–	–	–	–	–	–	65.03	0.28
Total	100.91	99.61883	99.72	98.81	99.87		98.37	99.54	99.5	100	99.62

as follows: Si (0.01), Na (0.03), F (0.05), Mg (0.02), Al (0.01), K (0.01) Mn (0.03), Zn (0.04), Ca (0.01), P (0.03), Ti (0.03), Cr (0.08), Cu (0.03), Zr (0.23), Y (0.15), Cl (0.02), S in silicates and sulfates (0.02), and Fe in silicates and sulfates (0.03). In addition to these, in-house standards were also measured to ensure measurements were consistent throughout data collection. Table 9 shows the chemistry of the dominant minerals in each simulant component determined by EMPA.

6.3. Raman spectroscopy

Raman spectroscopy was employed to confirm the mineralogy of the test samples using a Horiba Jobin-Yvon HR800 spectrometer. An Ar ion laser (at a wavelength of 514 nm) was used as the excitation source, which is a similar wavelength to that chosen by the European Space Agency for the Raman Laser Spectrometer (RLS) on board the ExoMars 2020 rover (Rull et al., 2017). Characterising the test samples using this laser allows for direct comparisons with the results from that mission. A 10% or 25% neutral density filter (N.D.) was used to reduce the power output of the laser to 0.7 mW and 0.9 mW, respectively, to prevent thermal heating of the sample that could potentially lead to changes in the Raman spectra.

A × 10 microscope objective was used to provide a spot size of 2.5 μm, and a 600 grooves per mm grating, which gives a spectral resolution of 1.5 cm^{-1}. A map of 100 or 200 spectra were taken over an area 1000 × 1000 μm for each of the components, with the exception of the phono-tephrite where individual point spectra of each constituent mineral phase were taken using a × 50 or × 100 microscope objective and an N.D. filter of 10% or 25% to ensure spectra were obtained.

Raman spectra were analysed using *Labspec* software, by first applying a baseline correction and then a peak fitting function using a Gaussian-Lorentzian profile to identify peak positions and peak widths. Minerals were identified by characteristic bands determined from existing literature and data obtained from the RRUFF project database (Lafuente et al., 2015). Table 10 shows characteristic peak positions of dominant mineral phases identified for simulant components.

6.4. X-ray fluorescence spectroscopy (XRF)

XRF was used to characterise the final simulants (four standard - OUXX-1 - and four with modified Fe^{2+} concentrations - OUXX-2). Subsamples from the <280 μm size fraction were further crushed using an agate ball mill to <63 μm crystal size for analysis. XRF was conducted by the University of Leicester on a PANalytical Axios-Advance X-ray fluorescence spectrometer using a 4 kW Rhodium anode end window ceramic technology X-ray tube. This provided quantitative chemical analysis of major and minor elements. Major elements were determined on fused glass beads, composed of sample material and lithium borate flux in a 1:5 ratio. Trace elements were determined on pressed powder briquettes

composed of sample powder and 12–15 drops of a 7% PVA solution (Moviol 8–88) pressed at 10 tons per sq. inch. Total loss on ignition (LOI), which liberates volatiles such as water, sulfur and chlorine, was measured on pre-dried powders through weighing before and after ignition at 950 °C in air for 1 h. Calibrations were set using international rock reference materials under the same conditions and regressing the measured count ratios against the recommended concentrations (Govindaraju, 1994; Imai et al., 1995, 1996, 1999) and values published on the GeoREM reference site, utilising the Philips based Fundamental parameters correction technique. Analytical precision (2σ) was determined utilising representative reference materials analysed during each run. Precision for the major oxides was typically ≤2%, and for trace elements was typically ≤5%. Results from XRF are given in Tables 11 and 12.

6.5. Sulfur analysis

Sulfur concentrations of all simulants were determined separately from other major and trace elements because some was lost during LOI determination. Therefore, sulfur analysis was conducted on subsamples of the <280 μm size fraction by AMG Superalloys (Rotherham, UK) using a LECO CS844 elemental analyser. Here, duplicates of each subsample were combusted to create SO_2, which was then measured using an infrared detector; the average results are reported on Table 13. The instrument was calibrated with certified pure/reference materials and additional certified reference materials (not used for calibration) were analysed alongside samples to validate results.

6.6. Mössbauer spectroscopy

To ascertain the Fe^{2+}/Fe^{3+} ratio of the simulants, transmission Mössbauer spectroscopy was conducted on subsamples of the <280 μm size fractions. Approximately 100 mg of these powdered samples were filled into acrylic glass holders with a circular area of ~1 cm^2. All Mössbauer spectra were obtained at room temperature using a standard Mössbauer transmission spectrometer (Wissel, Germany) with a ^{57}Co radiation source in constant acceleration mode. Spectra were calibrated against a spectrum of alpha-Fe foil (25 μm thickness) at room temperature and evaluated with Recoil (Ottawa, Canada) using the Voigt-based fitting routine (Rancourt and Ping, 1991). Instead of the natural linewidth, an experimental linewidth of 0.167 mm/s (taken at full width half maximum) was used which was determined as the linewidth of the innermost lines (third and fourth lines) in the alpha-Fe calibration spectrum. No f-factor correction was applied. Table 14 shows the Mössbauer data.

6.7. Physical properties

Characterisation of physical properties of all simulants (particle size,

Table 9
Microprobe analysis of dominant phases identified in simulant component materia.

	Dunite	Magnetite	Haematite (Haematite)	Haematite (Qtz)	FeSilicate	Apatite	Gypsum	Quartz	Wollastonite	Anorthosite (Albite)	Anorthosite (Zoisite)	Augite	Phono-tephrite (Feldspar)	Phono-tephrite (Leucite)	Phono-tephrite (Nosean)	Feldspar		Pyrite
SiO_2	41.99	0.02	0.20	101.29	37.50	1.03	0.00	101.11	51.43	64.63	39.60	46.43	59.38	54.84	36.97	53.91	**Si**	0.00
TiO_2	0.00	0.03	0.00	0.00	0.22	–	0.00	0.00	0.00	0.00	0.03	2.45	0.17	0.18	0.06	0.19	**Ti**	0.00
Al_2O_3	0.14	0.19	0.25	0.05	5.01	–	0.00	0.00	0.00	22.44	32.97	7.24	23.65	22.47	30.22	26.73	**Fe**	46.78
FeO^{a}	6.51	92.59	89.45	0.91	45.19	0.00	0.00	0.00	0.11	0.03	0.37	8.14	0.53	0.64	0.44	0.80	**Mn**	0.00
MnO	0.09	0.19	0.00	0.00	0.49	0.04	0.00	0.00	0.06	0.00	0.02	0.19	0.01	0.01	0.00	0.01	**Mg**	0.00
MgO	50.13	0.10	0.00	0.00	1.43	0.04	0.03	0.00	0.06	0.00	0.01	11.89	0.07	0.08	0.02	0.14	**Ca**	0.00
CaO	0.38	0.00	0.03	0.01	4.36	54.45	38.57	0.00	48.20	1.70	24.69	22.44	5.08	0.49	4.19	1.29	**K**	0.00
Na_2O	0.04	0.01	0.00	0.00	0.81	0.02	0.00	0.00	0.00	10.54	0.13	0.78	6.95	0.41	18.05	12.70	**S**	53.82
K_2O	0.02	0.00	0.00	0.00	0.47	–	0.00	0.00	0.00	0.10	0.00	0.11	2.66	19.84	2.79	3.98	**Cr**	0.00
P_2O_5	0.00	0.00	0.01	0.00	0.30	39.31	0.02	0.00	0.02	0.01	0.04	0.06	0.11	0.15	0.16	0.15	**Cu**	0.01
SO_3	0.00	0.00	0.05	0.01	0.90	–	52.49	0.00	0.00	0.01	0.00	0.00	0.01	0.09	6.72	0.09	**Zr**	0.00
SO_2	–	–	–	–	–	0.80	–	–	–	–	–	–	–	–	–	–		–
Cr_2O_3	0.04	0.00	0.00	0.00	0.26	–	0.00	0.00	0.00	0.00	0.00	0.02	–0.02	0.00	0.00	0.00		–
SrO	–	0.00	0.00	0.05	0.06	–	–	–	–	–	–	–	–	–	–	–		–
ZnO	–	0.10	0.00	0.00	1.88	–	–	–	–	–	–	–	–	–	–	–		–
CuO	–	0.00	0.00	0.00	0.65	–	–	–	–	–	–	–	–	–	–	–		–
F	–	–	–	–	–	4.18	–	–	–	–	–	–	–	–	–	–		–
Cl	–	–	–	–	–	0.09	–	–	–	–	–	–	–	–	–	–		–
Y_2O_3	–	–	–	–	–	0.03	–	–	–	–	–	–	–	–	–	–		–
Ce_2O_3	–	–	–	–	–	0.32	–	–	–	–	–	–	–	–	–	–		–
Total	99.35	93.11	89.83	102.30	99.53	100.31	91.05	101.09	99.89	99.46	97.88	99.76	98.59	99.19	99.62	99.97		100.53

a All Fe reported as FeO.

bulk density, porosity and particle shape) were conducted using washed subsamples of the 900-400 μm size fraction of each simulant and are shown in Tables 15 and 16.

Particle size distribution was determined using the wet sieve method, in accordance with BS 1377–2 1990 section 9 (by K4 soils, Watford, UK). Samples were oven dried and weighed, then passed through sieves with an aperture of 20 mm. The fraction of material that passed through each sieve was then weighed, spread into a tray and covered with water. After a minimum of 1 h, the material was washed through a nest of sieves with apertures of between 2 mm and 63 μm (aperture sizes are detailed in BS 1377–2 1990). Each resultant fraction was then dried and weighed to determine the mass fraction of each size. Fig. 3 shows the particle size distribution of each simulant.

One gram of subsample of each of the final simulants was taken and spread onto small trays. 100 grains of each were randomly selected and imaged using a Leica WILD MZ8 light microscope. From this, particle shape was determined using the particle shape classification scheme determined by Powers (1953), the results of which are illustrated in Table 15.

Bulk density estimates were determined for a subsample of the 900–400 μm size fraction using the linear measurement method (BS 1377–2, 1990 section 7; K4 soils, Watford, UK). Here, the sample of material was weighed and then poured into a mould. The internal dimensions of the mould were measured and the density (ρ) calculated using Equation (1):

$$\rho = 4000m/\left(\pi D^2 L\right) \tag{1}$$

where, m is mass in gram, D is mean diameter of cylinder and L is mean length.

Particle density was obtained using a small pyknometer (BS 1377–2 1990, section 8.3; K4 Soils, Watford, UK).

Porosity (n) was calculated from the bulk and particle density measurements by determining specific gravity (G_s) and void ratio (e) using Equations (2)–(4):

$$G_s = \rho_s/\rho_w \tag{2}$$

$$e = G_s(1+w)\frac{\rho_w}{\rho} - 1 \tag{3}$$

$$n = e/(1+e) \tag{4}$$

where, ρ_s is the particle density, ρ_w is the density of water ($1000\,\mathrm{kg\,m^{-3}}$), w is the water content (samples were dry samples) and ρ is bulk density.

7. Discussion

7.1. Component characteristics

The results of the SEM-EDS, EMPA and Raman analyses indicated that the components were not pure; in the case of dunite, anorthosite, apatite, magnetite, haematite, pyrite and wollastonite they contained additional or unexpected minerals and some minerals contained minor impurities (such as traces of Si within gypsum and metallic Cu within Fe-silicate glass) (Supplementary Table 1).

Although impure minerals were not ideal, they could be accommodated within the simulants because of the flexibility attributed by the use of individual components and the ability to adjust the chemistry accordingly. For example, quartz was detected as an additional mineral in four of the ten simulant components (anorthosite, wollastonite, apatite and haematite). This could have resulted in excess Si in the final simulants; however these components were used in smaller quantities than phono-tephrite and Fe-silicate glass, which provided the bulk of the Si, and so calculations and the final analysis of the products (see Section 6.2) demonstrated that the presence of quartz did not have a significant

Table 10

Raman peak positions of phases identified for each mineral identified in simulant components. Peak positions in bold identify the strongest and identifying peaks for each mineral.

Sample	Mineral	Average peak position (cm^{-1})									I.D. reference
Fe-silicate	Fe-silicate	**969**									Baert et al., 2011
Phono-tephrite	Leucite	**497**	**532**								Lafuente et al. (2015)
	Albite	**475**	**511**								Lafuente et al. (2015)
	Augite	330	392	**668**	1009						Huang et al. (2000)
Anorthosite	Albite	290	**480**	**508**	1100						Freeman et al. (2008); Lafuente et al. (2015)
	Zoisite	343	493	873	912	1073	1094	3154	3337		Lafuente et al. (2015)
Quartz	Quartz	129	208	265	357	**466**	514	812			Lafuente et al. (2015)
Dunite	Olivine	302	432	588	606	**824**	**856**	919	963	3685	Kuebler et al. (2006); Mouri and Enami (2008)
	Enstatite	342	**663**	**685**	1012	1031					Huang et al. (2000)
	Chromite	**563**	**685**								Lafuente et al. (2015)
Apatite	Apatite	432	584	**965**							Lafuente et al. (2015)
	Quartz	209	**465**								Lafuente et al. (2015)
Pyrite	Pyrite	**353**	**389**								López and Frost, 2015; Lafuente et al. (2015)
Magnetite	Magnetite	553	**676**								Lafuente et al. (2015)
	Augite	322	353	387	**666**	1014					Huang et al. (2000)
Gypsum	Gypsum	415	495	672	**1010**	1137	3404	3493			
Haematite	Haematite	228	296	415	503	617	1326				
	Quartz	207	**467**								Lafuente et al. (2015)
Wollastonite	Wollastonite	415	638	971							Lafuente et al. (2015)
	Diopside	233	325	358	391	561	**668**	**1015**			Huang et al. (2000)
	Gehlenite	641	698	867	**933**	3579					Lafuente et al. (2015)

Table 11

Major oxides (in wt%) for simulants as identified by XRF analysis.

	OUEB-1	OUSR-1	OUHR-1	OUCM-1	OUEB-2	OUSR-2	OUHR-1	OUCM-2
Na$_2$O	1.33	1.64	2.07	2.96	1.08	1.23	2.19	2.58
MgO	10.71	5.31	7.77	6.87	11.31	5.48	7.52	6.58
Al$_2$O$_3$	7.10	5.30	7.88	10.99	6.21	3.98	8.45	9.74
SiO$_2$	50.44	21.61	40.26	42.59	51.02	24.95	39.08	45.29
P$_2$O$_5$	0.52	3.25	0.61	0.73	0.54	3.14	0.65	0.68
SO$_3$	0.448	6.028	1.411	2.367	0.186	1.092	1.104	1.145
K$_2$O	0.71	1.31	1.46	2.18	0.55	0.95	1.53	1.87
CaO	9.52	9.20	6.55	7.95	10.18	8.33	6.57	7.63
TiO$_2$	0.28	0.51	0.56	0.83	0.20	0.40	0.60	0.75
Cr$_2$O$_3$	0.179	0.065	0.111	0.122	0.160	0.049	0.137	0.077
MnO	0.19	0.11	0.19	0.21	0.06	0.25	0.15	
Fe$_2$O$_3$[a]	19.32	36.48	30.93	22.52	18.80	34.55	29.26	22.19
LOI	−1.10	8.15	−0.84	−1.30	−0.33	14.19	1.32	−0.05
Total	100.73	99.75	99.94	100.06	101.31	98.96	99.31	99.34

[a] All Fe reported as Fe$_2$O$_3$.

impact. The mineral quartz was used to fine-tune the Si concentration, where required. Further, the presence of some additional minerals (e.g. pyroxenes, actinolite, chlorite) within the simulant components meant the simulant mineralogy was more realistic to the martian regolith (Table 5). The final proportions of minerals used in the simulants, and the expected simulant chemistries, are those given in Tables 6 and 7

7.2. Simulant characteristics

7.2.1. Chemistry

In order to produce a final, defined chemistry for each simulant, based on the analyses conducted, elemental sulfur concentrations obtained from the sulfur analysis were converted to oxides (SO$_3$). These were then substituted into the XRF data, since the sulfur data from the XRF was determined to be inaccurate because of the LOI step in the analysis. Further, since the XRF analysis did not provide Fe speciation, the total Fe was partitioned into Fe^{2+} and Fe^{3+} as determined by Mössbauer analysis. The data was then normalised (Table 17).

OUCM-2, OUEB-1 and -2 had chemistries within 2 wt% of their targets. OUCM-1 was within 3 wt% for each oxide, and OUHR-1 and -2 were within 4 wt%. OUSR-1 and -2 showed the greatest variation (up to 6 wt %) when compared to the target martian chemistries. However, these variations are specifically accounted for by SO$_3$ (for both OUSR-1 and -2) and SiO$_2$ (for OUSR-1). OUSR-1 and -2 also had higher concentrations of sulfur than intended (5.8 and 5.9 wt% higher respectively), possibly resulting from minerals such as gypsum and pyrite that may have contained more sulfur than was determined in the component characterisation. OUSR-1 also had a lower SiO$_2$ (5.3 wt% lower than target), potentially resulting from heterogeneities in the apatite and phono-tephrite used. However, MSL's APXS has revealed a sulfur-rich (40.78 wt%) and silica poor (14.41 wt%) deposit, Indianola, at Gale Crater (Gellert, 2013). Therefore, OUSR-1 and -2 are still representative of sulfur rich material found on Mars, as sulfur and silica concentrations are within the range of those identified in similar deposits found on Mars.

Although total Fe was within 5 wt% for each simulant, the Mössbauer data revealed that the partitioning of Fe^{2+} and Fe^{3+} was not as expected in all simulants: Fe^{2+} was present at higher concentrations (7% of total Fe) than intended. However, OUSR-2 had a concentration of Fe^{2+} that was 20% (of total Fe) higher than required. This simulant had originally been intended to contain a 50:50 partitioning of Fe^{2+}:Fe^{3+}, with the

Table 12
Trace elements (in ppm) for simulants as determined by XRF analysis.

	OUEB-1	OUSR-1	OUHR-1	OUCM-1	OUEB-2	OUSR-2	OUHR-2	OUCM-2
As	24.1	28.9	33.8	23.7	22.7	25.7	31.8	22.7
Ba	900.6	685.6	1552.8	1180.9	1155.5	987.1	1102.5	1554.2
Ce	76.9	188.2	81.1	114.4	60.7	202.6	93.2	98.5
Co	127.7	66.8	80.4	117.8	77.6	30.6	129.4	59.2
Cr	1039.6	404.8	564.3	745.5	789.9	200.0	918.0	394.2
Cs	<1.6	2.9	<1.6	<1.7	<1.7	<2.1	<1.6	<1.8
Cu	4020.7	929.9	1823.1	3311.4	1281.2	87.6	4468.3	810.9
Ga	10.5	11.3	13.1	17.2	7.9	8.7	15.3	13.7
La	47.5	95.7	49.6	70.0	32.8	104.2	59.3	63.6
Mo	619.1	173.5	347.5	535.6	276.1	5.9	647.8	185.3
Nb	19.5	41.8	42.5	56.9	20.7	49.0	41.6	59.8
Nd	22.5	60.1	24.2	37.0	18.5	62.8	28.8	30.9
Ni	607.7	392.0	411.0	351.5	600.6	275.1	512.2	274.9
Pb	77.9	77.1	58.3	74.3	37.2	50.2	90.2	34.5
Rb	26.3	53.2	53.5	69.9	26.6	61.8	52.3	73.3
Sb	47.1	17.2	35.1	50.0	29.2	3.2	57.3	24.2
Sc	3.4	2.6	5.7	5.4	5.8	7.1	4.0	7.8
Se	<1.1	2.6	3.4	<1.1	1.1	1.5	<1.3	<1.0
Sn	624.2	220.7	353.3	593.7	302.2	18.6	699.1	205.3
Sr	344.4	507.6	557.4	694.2	349.5	581.3	543.0	719.3
Th	21.2	103.5	23.4	24.1	19.7	107.5	24.1	25.1
U	5.6	7.0	6.0	6.1	3.9	6.5	7.1	4.8
V	44.0	67.7	66.9	94.7	42.3	83.6	70.6	101.6
W	27.8	91.4	24.8	32.4	11.4	70.6	42.2	12.2
Y	14.9	26.2	15.5	21.1	10.9	25.7	19.6	16.8
Zn	7669.4	2170.9	3669.5	6419.3	2530.1	300.9	8653.7	1641.9
Zr	223.3	176.8	221.8	321.6	132.6	154.7	300.5	235.9

Table 13
Sulfur concentration as determined by elemental analysis.

	S abundance (%)							
	OUEB -1	OUSR-1	OUHR-1	OUCM-1	OUEB -2	OUSR-2	OUHR -2	OUCM -2
Target	0.20	12.69	1.87	2.22	0.20	12.69	1.87	2.22
Simulant	0.16	19.67	3.55	2.30	0.18	19.26	3.55	2.48

Table 14
Fe speciation as determined by Mössbauer analysis (in percent).

	OUEB-1	OUSR-1	OUHR-1	OUCM-1	OUEB-1	OUSR-2	OUHR-2	OUCM-2
Pyroxene Site A (Fe^{2+})	26	3	8	30	13	1	18	13
Pyroxene Site B (Fe^{2+})	41	14	26	31	19	1	50	21
Olivine (Fe^{2+})	17	3	7	12	18	2	8	6
Fe^{3+}	9	2	3	4	7	0	5	3
Pyrite (Fe^{2+})	0	67	13	11	0	82	8	13
Magnetite ($Fe^{2.5+}$)	4	7	6	7	5	0	5	7
Magnetite (Fe^{3+})	3	5	4	5	3	0	4	6
Haematite (Fe^{3+})	0	0	33	0	35	13	2	32
Total Fe^{2+}	**86.0**	**90.5**	**57.0**	**87.5**	**52.5**	**86.0**	**86.5**	**56.5**
Total Fe^{3+}	**14.0**	**10.5**	**43.0**	**12.5**	**47.5**	**13.0**	**13.5**	**44.5**

majority of Fe being supplied by pyrite. Pyrite was also used to provide the required S for this S-enriched simulant, so to achieve the required S concentrations, 40% of the simulant was pyrite. As a consequence, OUSR-2 contained more Fe^{2+} than intended (approx. 5 wt%). To mitigate this, Fe-silicate glass and magnetite, other sources of Fe^{2+}, were removed from OUSR-2, and substituted by haematite. However, the sample of haematite used for the final simulant may have contained more SiO_2 than was determined in the test sample. This would have reduced its Fe^{3+} contribution, resulting in a higher Fe^{2+}/Fe^{3+} ratio than expected.

Given this difference in Fe^{2+}/Fe^{3+} ratio compared to the target chemistry, we cannot state with confidence that OUSR-1 can be modified to reflect the variety of Fe chemistries for Paso Robles-type S-rich regolith reported by other studies (Gellert et al., 2013a; Gellert et al., 2006). However, OUCM-1 and -2, OUHR-1 and -2, and OUEB-1 and -2 are within the acceptable compositional range (±5 wt%) of the martian chemistries they intended to simulate and can be modified to reflect variable Fe chemistry. Further, the compositional match between the simulants

presented in this study (with the exception of OUSR-2) and their target chemistries is closer than that achieved by pre-existing simulants (Table 3). The CRB is the only pre-existing analogue (or simulant) with a chemistry of within 5 wt% of the average global martian regolith chemistry; our equivalents (OUCM-1 and -2) are within 3 wt %.

7.2.2. Physical properties

Although not originally defined to be physically similar to the martian regolith, it is important to report physical properties that may have an impact on the simulants' future uses. For example, the bulk density and porosity of soils will influence their mechanical and thermal properties and affect experiments exploring, for example, thermal measurements, wind drift and gas diffusion (Hudson et al., 2007; Seiferlin et al., 2008).

Given the size fraction characterised (900-400 μm), it is unsurprising that they could all be classified as sands (2000-200 μm) (Fig. 3). All contain a proportion of grains <300 μm, particularly OUSR-1 and -2. This may be attributable to the break-up of gypsum along cleavage planes

Table 15
Particle shape and sphericity classification.

		Abundance (%)					
		Very angular	Angular	Sub-angular	Sub-rounded	Rounded	Well-rounded
OUCM -1	High sphericity	5	7	13	1	6	2
	Low sphericity	13	8	10	31	4	0
	Total	*18*	*15*	*23*	*32*	*10*	*2*
OUSR-1	High sphericity	14	10	5	0	0	1
	Low sphericity	18	13	11	28	0	0
	Total	*32*	*23*	*16*	*28*	*0*	*1*
OUHR-1	High sphericity	5	4	16	2	0	0
	Low sphericity	11	10	20	32	0	0
	Total	*16*	*14*	*36*	*34*	*0*	*0*
OUEB-1	High sphericity	2	3	17	2	1	2
	Low sphericity	15	9	10	36	3	0
	Total	*17*	*12*	*27*	*38*	*4*	*2*
OUCM-2	High sphericity	4	7	9	1	1	0
	Low sphericity	11	10	19	36	2	0
	Total	*15*	*17*	*28*	*37*	*3*	*0*
OUSR-2	High sphericity	11	2	4	0	3	0
	Low sphericity	20	14	12	33	1	0
	Total	*31*	*16*	*16*	*33*	*4*	*0*
OUHR-2	High sphericity	2	3	6	1	5	5
	Low sphericity	11	18	15	33	1	0
	Total	*13*	*21*	*21*	*34*	*6*	*5*
OUEB-2	High sphericity	6	6	9	2	1	0
	Low sphericity	13	11	19	32	1	0
	Total	*19*	*17*	*28*	*34*	*2*	*0*

Table 16
Physical properties of simulants.

	OUEB-1	OUSR-1	OUHR-1	OUCM-1	OUEB-2	OUSR-2	OUHR-2	OUCM-2
Bulk density (kg m^{-3})	1580	1950	1620	1630	1560	1810	1660	1570
Particle density (kg m^{-3})	3150	3720	3350	3230	3150	3570	3340	3160
Porosity (%)	49.8	47.7	51.7	49.6	50.5	49.2	50.3	50.4
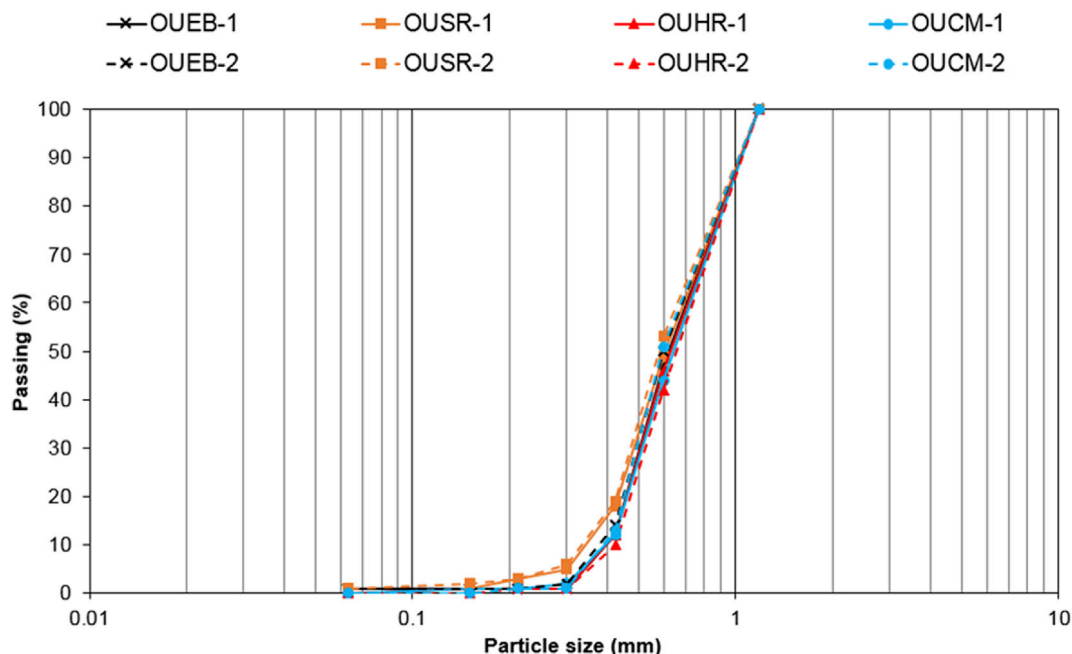
Fig. 3. Grain size distribution for each simulant using the 900-400 μm size fraction.

during the mixing or analysis processes, or because washing did not remove all the fine-grained material. The <300 μm size fraction represented, at most, only 6% of each individual simulant, and so did not affect the overall grain size classification.

Grain shape in all simulants was predominantly very angular to sub-angular (56–71% of grains), with a low sphericity (66–80% of grains). OUSR-1 and -2 have 32% and 31% (respectively) very angular grains, likely because these simulants contain more pyrite (40 wt%) (Fig. 4). However, OUCM-1, OUSR-1 and -2, and OUEB-1 have particles classified as well-rounded with high sphericity; these grains were Fe-silicate glass

Table 17
Combined chemical data (normalised).

	OUEB -1	OUSR-1	OUHR-1	OUCM-1	OUEB -2	OUSR-2	OUHR -2	OUCM -2
Na_2O	1.35	1.25	1.96	2.91	1.08	0.96	2.13	2.51
MgO	10.82	4.06	7.36	6.76	11.35	4.29	7.33	6.40
Al_2O_3	7.17	4.05	7.47	10.80	6.23	3.11	8.24	9.48
SiO_2	50.93	16.50	38.17	41.87	51.21	19.51	38.10	44.11
P_2O_5	0.52	2.48	0.58	0.72	0.54	2.45	0.63	0.66
SO_3[a]	0.40	37.50	8.40	5.65	0.45	37.60	8.64	6.03
K_2O	0.71	1.00	1.38	2.14	0.55	0.74	1.49	1.82
CaO	9.61	7.03	6.21	7.82	10.22	6.52	6.41	7.43
TiO_2	0.28	0.39	0.53	0.81	0.20	0.31	0.58	0.73
Cr_2O_3	0.18	0.05	0.11	0.12	0.16	0.04	0.13	0.08
MnO	0.20	0.08	0.18	0.21	0.12	0.04	0.25	0.14
FeO	15.10	22.68	15.04	17.43	8.91	20.91	22.20	10.99
Fe_2O_3	2.73	2.92	12.61	2.77	8.96	3.51	3.85	9.62
Total	100.00	100.00	100.00	100.00	100.00	100.00	100.00	100.00

[a] SO_3 determined by S gas analysis using a LECO instrument.
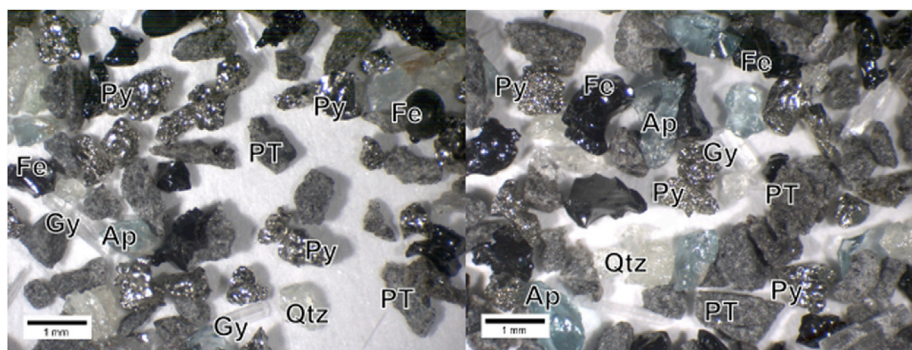
Fig. 4. Examples of angular grains of pyrite taken from OUSR-1. For clarity, examples of grains have been labelled: Py - pyrite, PT - phono-tephrite, Fe – Fe-silicate glass, Gy - gypsum, Qtz - quartz and Ap - apatite.

particles (Fig. 5) and their shape is presumably the result of quenching during the smelting process. Grain shapes on Mars are seen to vary according to provenance or soil type, i.e., in ripples, plains or dunes (Cabrol et al., 2008; Weitz et al., 2006, 2018) but the overall particle shape was sub-rounded to rounded, and elongated, suggesting extensive abrasion (Cabrol et al., 2008; Weitz et al., 2018). This is contrary to the simulants presented here (and previous simulants, Peters et al., 2008; Scott et al., 2017; Zeng et al., 2015), but is unavoidable since these simulants were mechanically crushed, generating high angularity. Particle shape can be used to determine properties such as friction angle and cohesion, which are used to predict rover locomotion performance (Brunskill et al., 2011). However, to fully determine the suitability of these simulants for such engineering purposes further testing would be required, which is beyond the scope of this paper.

Bulk densities of these simulants are presented in Table 15. OUSR-1

and -2 have the highest bulk densities (1.95 and 1.81 g cm^{-3}, respectively), whereas OUEB-1 and -2 have the lowest (1.58 and 1.56 g cm^{-3}, respectively). Estimates made at the Viking landing sites ranged from 0.57 g cm^{-3} to 1.60 g cm^{-3} (Clark et al., 1976; Moore and Jakosky, 1989; Moore et al., 1987; Shorthill et al., 1976), with Pathfinder landing site estimates increasing the range of bulk densities on the martian surface to 2 g cm^{-3} (Golombek et al., 1997). Thus, the simulants presented in this paper fall within the range of possible bulk densities for the martian regolith and could be suitable for some engineering applications. They may be particularly useful for applications that require the mechanical insertion of an instrument package into the regolith for measurement (e.g., Richter et al., 2002).

Calculated porosities for the final simulants are between 47 and 52% (Table 15); OUHR-1 has the highest porosity (51.7%) and OUSR-1 the lowest (47.7%). Although the porosity of the martian regolith is poorly
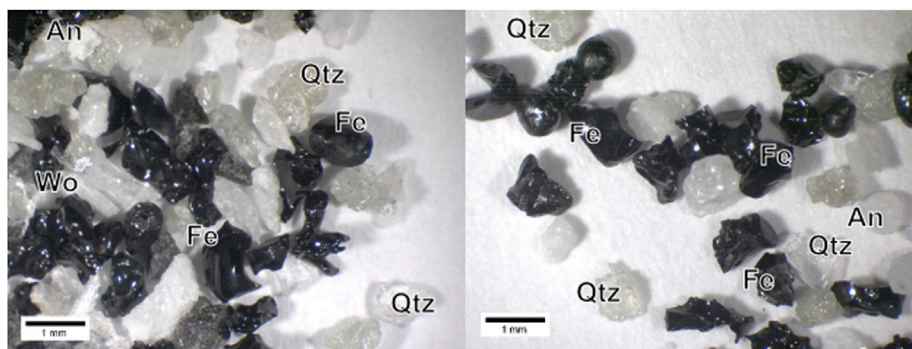
Fig. 5. Examples of spherical grains of Fe-silicates glass taken from OUEB-1. For clarity, examples of grains have been labelled: Fe – Fe-silicate glass, Qtz - quartz, Wo - wollastonite and An - anorthosite.

known, estimates inferred from the same samples that were analysed by Viking's XRF suggested that porosity was between 31 and 58% (assuming a grain density of $2.6 \, g \, cm^{-3}$ and bulk densities between 1.10 and $0.57 \, g \, m^{-3}$; Moore and Jakosky, 1989), and wind drift material could have porosities as high as 60% (Clark et al., 1976). As with bulk density, the porosities determined for these simulants fall within the range estimated for Mars.

8. Summary and conclusions

Eight simulants have been produced that are representative of various chemical environments on Mars. Four of these are representative of measured martian chemistry, with the other four possessing modified Fe^{2+}/Fe^{3+} ratios. Where possible, minerals were used that are equivalent to those found on the martian surface.

The chemistries and mineralogies of the simulant components were characterised by SEM-EDS, EPMA and Raman, and the final simulants characterised by Mössbauer, XRF and S elemental analysis. Selected physical properties of the final simulants were characterised including bulk and particle density, porosity, grain size and shape. All simulants are, on the whole, chemically equivalent (within ~5 wt%) to the martian chemistries on which they were based. Unlike previous simulants or analogues, they possess Fe^{2+} concentrations equivalent to those believed to exist on Mars and, with the exception of OUSR-1, these simulants can be modified to adjust their Fe^{2+} concentrations without disrupting their overall chemistry (represented by OUXX-2 simulants here).

Although mimicking the physical properties of the martian regolith was not a requirement for these simulants, characterisation of one of the grain size fractions (900-400 μm) for each simulant has been undertaken and the bulk density and porosity of this grain size fraction is comparable to estimates for the martian regolith.

The simulants are suitable for a range of investigations that depend on simulating martian chemistry. Experiments are under way using these to investigate water-rock and water-rock-microbe relationships with a variety of species, and the role of Fe^{2+}/Fe^{3+} variation. They may also be used to investigate the production of chemical biosignatures, or investigations for which the bulk density and porosity are relevant, such as gas diffusion experiments or ice formation within the regolith pore spaces.

Whilst these simulants have been made with astrobiological laboratory simulation experiments in mind, they have been made in sufficient quantities that they can be made available for further projects, upon request. In addition, they have been made in such a way that they can be reproduced using the component proportions identified in this paper. This should allow for cross-study and inter-laboratory comparisons to understand local and global martian geochemistry, as well as other characteristics such as habitability, which can and aid the interpretation of data returned from current and future missions to Mars.

Acknowledgements

Appendix A. Supplementary data

Supplementary data to this article can be found online at https://doi.org/10.1016/j.pss.2019.104722.

Supplementary Table 1 Mineral phases identified for each component used to make simulants, as determined by SEM-EDS, Raman spectroscopy and EMPA.

Sample	Form	Dominant phase(s)	Additional phases	Notes
Phono-tephrite	Large specimens (approx.10 cm in length)	Feldspathoid (30%) Plagioclase feldspar (30%) Augite (35%).	Titanomagnetite (5%)	Augite found as phenocrysts enclosed in feldspar/feldspathoid matrix.
Fe-silicate glass	Grains (<3 mm)	Fe-silicate glass (99%)	Metallic copper (<1%)	Two distinct phases, a dark dominant phase with particulates of a bright phase attached. The dark phase is rich in Si and Fe, with minor amounts of Ca, Mg and Zn (between 1 and 5 wt %). Bright phases are metallic Cu.
Anorthosite	Hand specimen (3–6 cm in length)	Albite (46%) and Zoisite, (50%)	Paragonite (2%) Quartz (2%) Anorthite (<1%)	
Quartz	Hand specimen	Quartz (100%)		
Dunite	Hand specimen (3–6 cm in length)	Olivine-Fo$_{0.93}$ (94%)	Enstatite (4%), chromite (1%) and chlorite (1%)	Chlorite around enstatite grains, some hydration of olivine.
Apatite	Large specimen (approx.20 cm in length)	Fluorapatite (92%)	Quartz (8%)	Apatite contained approximately 4 wt% F.
Pyrite	Hand specimen (3–6 cm in length)	Pyrite (99%)	Tennantite, covellite, tenorite, dolomite and anhydrite (in total <1%).	Additional trace minerals and a phase rich in Ca, P and Mg. Traces of CuO (<0.5%)
Magnetite	Hand specimen (3–6 cm in length)	Magnetite (85%)	Augite (~11%), Epidote (2%), Chlorite (<1%) Pargasite (<1%) and actinolite (<1%).	High concentration of Ca along a fracture. Sample likely to have undergone some aqueous alteration.
Gypsum	Hand specimen (3–6 cm in length)	Gypsum (100%)		Traces of silica (<2 wt%), but no quartz.
Haematite	Hand specimen (3–6 cm in length)	Haematite (80%) quartz (20%)		Trace amounts of Al (<1 wt %)
Wollastonite	Grains (<5 mm)	Wollastonite (82%)	Quartz, (10%) Diopside (3%) Gehlenite (5%)	Features rich in Ca (80–81 wt%)

References

Nockolds, S.R., 1954. Average chemical compositions of some igneous rocks. Geol. Soc. Am. Bull. 65 (1007). https://doi.org/10.1130/0016-7606(1954)65[1007:ACCOSI]2.0.CO;2.

Allen, C.C., Jager, K.M., Morris, R.V., Lindstrom, D.J., Lindstrom, M.M., Lockwood, J.P., 1998a. Martian soil simulant available for scientific, educational study. Eos, Trans. Am. Geophys. Union 79, 405–405. https://doi.org/10.1029/98EO00309.

Allen, C.C., Morris, R.V., Jager, K.M., Golden, D.C., Lindstrom, D.J., Lindstrom, M.M., Lockwood, J.P., Martin, L., 1998b. Martian Regolith Simulant JSC Mars-1, Lunar and Planetary Science Conference. Abstrat# 1690.

Amils, R., Fernández-Remolar, D., IPBSL Team, 2014. Río Tinto: a geochemical and mineralogical terrestrial analogue of mars. Life 4, 511–534. https://doi.org/10.3390/life4030511.

Baert, K., Meulebroeck, W., Wouters, H., Cosyns, P., Nys, K., Thienpont, H., Terryn, H., 2011. Using Raman spectroscopy as a tool for the detection of iron in glass. J. Raman Spectrosc. 42, 1789–1795. https://doi.org/10.1002/jrs.2935.

Baker, L.L., Agenbroad, D.J., Wood, S.A., 2000. Experimental hydrothermal alteration of a martian analog basalt: implications for martian meteorites. Meteorit. Planet. Sci. 35, 31–38. https://doi.org/10.1111/j.1945-5100.2000.tb01971.x.

Baqué, M., Verseux, C., Böttger, U., Rabbow, E., de Vera, J.P.P., Billi, D., 2016. Preservation of biomarkers from cyanobacteria mixed with mars-like regolith under simulated martian atmosphere and UV flux. Orig. Life Evol. Biosph. 46, 289–310. https://doi.org/10.1007/s11084-015-9467-9.

Bauermeister, A., Rettberg, P., Flemming, H.C., 2014. Growth of the acidophilic iron-sulfur bacterium Acidithiobacillus ferrooxidans under Mars-like geochemical conditions. Planet. Space Sci. 98, 205–215. https://doi.org/10.1016/j.pss.2013.09.009.

Bibring, J.P., Langevin, Y., Gendrin, A., Gondet, B., Poulet, F., Berthé, M., Soufflot, A., Arvidson, R.E., Mangold, N., Mustard, J., Drossart, P., Team, the O, 2005. Mars surface diversity as revealed by the OMEGA/mars express observations. Science 307, 1576–1581. https://doi.org/10.1126/science.1108806.

Bish, D.L., Blake, D.F., Vaniman, D.T., Chipera, S.J., Morris, R.V., Ming, D.W., Treiman, A.H., Sarrazin, P., Morrison, S.M., Downs, R.T., Achilles, C.N., Yen, A.S., Bristow, T.F., Crisp, J.A., Morookian, J.M., Farmer, J.D., Rampe, E.B., Stolper, E.M., Spanovich, N., MSL Team, 2014. X-ray diffraction results from mars. Science 341, 1–6. https://doi.org/10.1126/science.1238932.

Bishop, J.L., Rampe, E.B., 2016. Evidence for a changing martian climate from the mineralogy at Mawrth Vallis. Earth Planet. Sci. Lett. 448, 42–48. https://doi.org/10.1016/J.EPSL.2016.04.031.

Blake, D.F., Morris, R.V., Kocurek, G., Morrison, S.M., Downs, R.T., Bish, D., Ming, D.W., Edgett, K.S., Rubin, D., Goetz, W., Madsen, M.B., Sullivan, R., Gellert, R., Campbell, I., Treiman, A.H., McLennan, S.M., Yen, A.S., Grotzinger, J., Vaniman, D.T., Chipera, S.J., Achilles, C.N., Rampe, E.B., Sumner, D., Meslin, P.Y., Maurice, S., Forni, O., Gasnault, O., Fisk, M., Schmidt, M., Mahaffy, P., Leshin, L.A., Glavin, D., Steele, A., Freissinet, C., Navarro-González, R., Yingst, R.A., Kah, L.C., Bridges, N., Lewis, K.W., Bristow, T.F., Farmer, J.D., Crisp, J.A., Stolper, E.M., Des Marais, D.J., Sarrazin, P., 2013. Curiosity at Gale crater, mars: characterization and analysis of the rocknest sand shadow. Science 341, 1–8. https://doi.org/10.1126/science.1239505.

Bost, N., Westall, F., Ramboz, C., Foucher, F., Pullan, D., Meunier, A., Petit, S., Fleischer, I., Klingelhöfer, G., Vago, J.L., 2013. Missions to mars: characterisation of mars analogue rocks for the international space analogue Rockstore (ISAR). Planet. Space Sci. 82–83, 113–127. https://doi.org/10.1016/j.pss.2013.04.006.

Böttger, U., De Vera, J.P., Fritz, J., Weber, I., Hübers, H.W., Schulze-Makuch, D., 2012. Optimizing the detection of carotene in cyanobacteria in a martian regolith analogue with a Raman spectrometer for the ExoMars mission. Planet. Space Sci. 60, 356–362. https://doi.org/10.1016/j.pss.2011.10.017.

Bridges, J.C., Schwenzer, S.P., 2012. The nakhlite hydrothermal brine on Mars. Earth Planet. Sci. Lett. 359–360, 117–123. https://doi.org/10.1016/J.EPSL.2012.09.044.

Bridges, J.C., Warren, P.H., 2006. The SNC meteorites: basaltic igneous processes on Mars. J. Geol. Soc. London. 163, 229–251. https://doi.org/10.1144/0016-764904-501.

Bristow, T.F., Rampe, E.B., Achilles, C.N., Blake, D.F., Chipera, S.J., Craig, P., Crisp, J.A., Des Marais, D.J., Downs, R.T., Gellert, R., Grotzinger, J.P., Gupta, S., Hazen, R.M., Horgan, B., Hogancamp, J.V., Mangold, N., Mahaffy, P.R., McAdam, A.C., Ming, D.W., Morookian, J.M., Morris, R.V., Morrison, S.M., Treiman, A.H., Vaniman, D.T., Vasavada, A.R., Yen, A.S., 2018. Clay mineral diversity and abundance in sedimentary rocks of Gale crater, Mars. Sci. Adv. 4 eaar3330. https://doi.org/10.1126/sciadv.aar3330.

Brunskill, C., Patel, N., Gouache, T.P., Scott, G.P., Saaj, C.M., Matthews, M., Cui, L., 2011. Characterisation of martian soil simulants for the ExoMars rover testbed. J. Terramechanics 48, 419–438. https://doi.org/10.1016/j.jterra.2011.10.001.

BS 1377-7, 1990. Soils for civil engineering purposes. Br. Stand. Inst. 3.

Cabrol, N.A., Herkenhoff, K.E., Greeley, R., Grin, E.A., Schröder, C., d'Uston, C., Weitz, C., Yingst, R.A., Cohen, B.A., Moore, J., Knudson, A., Franklin, B., Anderson, R.C., Li, R., 2008. Soil sedimentology at Gusev Crater from Columbia Memorial station to winter haven. J. Geophys. Res. E Planets 113, 1–11. https://doi.org/10.1029/2007JE002953.

Calvin, W.M., Shoffner, J.D., Johnson, J.R., Knoll, A.H., Pocock, J.M., Squyres, S.W., Weitz, C.M., Arvidson, R.E., Bell, J.F., Christensen, P.R., de Souza, J.A., Farrand, W.H., Glotch, T.D., Herkenhoff, K.E., Jolliff, B.L., Knudson, A.T., McLennan, S.M., Rogers, A.D., Thompson, S.D., 2008. Hematite spherules at Meridiani: results from MI, Mini-TES, and Pancam. J. Geophys. Res. E Planets 113. https://doi.org/10.1029/2007JE003048.

Cannon, K.M., Britt, D.T., Smith, T.M., Fritsche, R.F., Batcheldor, D., 2019. Mars global simulant MGS-1: a Rocknest-based open standard for basaltic martian regolith simulants. Icarus 317, 470–478. https://doi.org/10.1016/J.ICARUS.2018.08.019.

Carr, M.H., Head, J.W., 2010. Geologic history of mars. Earth Planet. Sci. Lett. 294, 185–203. https://doi.org/10.1016/j.epsl.2009.06.042.

Carrizo, D., Sánchez-García, L., Gómez, F., 2018. Molecular evidences of life in a poly-extreme environment in Ethiopia, the Dallol Hot Springs area, based on lipidic biomarkers. In: European Planetary Science Conference. EPSC2018–E2044.

Carter, J., Poulet, F., Bibring, J.P., Mangold, N., Murchie, S., 2013. Hydrous minerals on Mars as seen by the CRISM and OMEGA imaging spectrometers: updated global view. J. Geophys. Res. E Planets 118, 831–858. https://doi.org/10.1029/2012JE004145.

Carter, J., Loizeau, D., Mangold, N., Poulet, F., Bibring, J.-P., 2015. Widespread surface weathering on early Mars: a case for a warmer and wetter climate. Icarus 248, 373–382. https://doi.org/10.1016/J.ICARUS.2014.11.011.

Chastain, B.K., Kral, T.A., 2010. Approaching Mars-like geochemical conditions in the laboratory: omission of artificial buffers and reductants in a study of biogenic methane production on a smectite clay. Astrobiology 10, 889–897. https://doi.org/10.1089/ast.2010.0480.

Christensen, P.R., Bandfield, J.L., Clark, R.N., Edgett, K.S., Hamilton, V.E., Hoefen, T., Kieffer, H.H., Kuzmin, R.O., Lane, M.D., Malin, M.C., Morris, R.V., Pearl, J.C., Pearson, R., Roush, T.L., Ruff, S.W., Smith, M.D., 2000. Detection of crystalline hematite mineralization on mars by the thermal emission spectrometer: evidence for near-surface water. J. Geophys. Res. E Planets 105, 9623–9642. https://doi.org/10.1029/1999JE001093.

Cino, C.D., Dehouck, E., McLennan, S.M., 2017. Geochemical constraints on the presence of clay minerals in the Burns formation, Meridiani Planum, Mars. Icarus 281, 137–150. https://doi.org/10.1016/j.icarus.2016.08.029.

Clark, B.C., Baird, A.K., Rose, H.J., Toulmin, P., Keil, K., Castro, A.J., Kelliher, W.C., Rowe, C.D., Evans, P.H., 1976. Inorganic analyses of Martian surface samples at the Viking landing sites. Science 194, 1283–1288. https://doi.org/10.1126/science.194.4271.1283.

Clark, B.C., Baird, a.K., Weldon, R.J., Tsusaki, D.M., Schnabel, L., Candelaria, M.P., 1982. Chemical composition of Martian fines. J. Geophys. Res. 87, 10059–10067. https://doi.org/10.1029/JB087iB12p10059.

Clark, B.C., Morris, R.V., McLennan, S.M., Gellert, R., Jolliff, B., Knoll, A.H., Squyres, S.W., Lowenstein, T.K., Ming, D.W., Tosca, N.J., Yen, A., Christensen, P.R., Gorevan, S., Brückner, J., Calvin, W., Dreibus, G., Farrand, W., Klingelhoefer, G., Waenke, H., Zipfel, J., Bell, J.F., Grotzinger, J., McSween, H.Y., Rieder, R., 2005. Chemistry and mineralogy of outcrops at Meridiani Planum. Earth Planet. Sci. Lett. 240, 73–94. https://doi.org/10.1016/j.epsl.2005.09.040.

Cloutis, E.A., Mann, P., Izawa, M.R.M., Applin, D.M., Samson, C., Kruzelecky, R., Glotch, T.D., Mertzman, S.A., Mertzman, K.R., Haltigin, T.W., Fry, C., 2015. The Canadian space agency planetary analogue materials suite. Planet. Space Sci. 119, 155–172. https://doi.org/10.1016/j.pss.2015.09.001.

Deer, W.A., Howie, R.A., Zussman, J., 1992. An Introduction to the Rock-Forming Minerals. Longman Scientific & Technical.

Dehouck, E., Gaudin, A., Chevrier, V., Mangold, N., 2016. Mineralogical record of the redox conditions on early Mars. Icarus 271, 67–75. https://doi.org/10.1016/J.ICARUS.2016.01.030.

Ding, S., Dasgupta, R., Lee, C.T.A., Wadhwa, M., 2015. New bulk sulfur measurements of Martian meteorites and modeling the fate of sulfur during melting and crystallization - implications for sulfur transfer from Martian mantle to crust-atmosphere system. Earth Planet. Sci. Lett. 409, 157–167. https://doi.org/10.1016/j.epsl.2014.10.046.

Edwards, P.H., Bridges, J.C., Wiens, R., Anderson, R., Dyar, D., Fisk, M., Thompson, L., Gasda, P., Filiberto, J., Schwenzer, S.P., Blaney, D., Hutchinson, I., 2017. Basalt-trachybasalt samples in Gale crater, mars. Meteorit. Planet. Sci. 52, 2931–2410. https://doi.org/10.1111/maps.12953.

Ehlmann, B.L., Edwards, C.S., 2014. Mineralogy of the martian surface. Annu. Rev. Earth Planet Sci. 42, 291–315. https://doi.org/10.1146/annurev-earth-060313-055024.

Fackrell, P.L.E., 2018. Development of Martian Regolith Simulants for Exploration of in Situ Resource Availability and Potential, Lunar and Planetar Science Conference. Abstract# 2742.

Fergason, R.L., Gaddis, L.R., Rogers, A.D., 2014. Hematite-bearing materials surrounding candor Mensa in candor Chasma, mars: implications for hematite origin and post-emplacement modification. Icarus 237, 350–365. https://doi.org/10.1016/j.icarus.2014.04.038.

Filiberto, J., 2017. Geochemistry of Martian basalts with constraints on magma genesis. Chem. Geol. 466, 1–14. https://doi.org/10.1016/J.CHEMGEO.2017.06.009.

Foley, C.N., Economou, T., Clayton, R.N., 2003. Final chemical results from the Mars Pathfinder alpha proton X-ray spectrometer. J. Geophys. Res. Planets 108. https://doi.org/10.1029/2002JE002019.

Fraeman, A.A., Arvidson, R.E., Catalano, J.G., Grotzinger, J.P., Morris, R.V., Murchie, S.L., Stack, K.M., Humm, D.C., McGovern, J.A., Seelos, F.P., Seelos, K.D., Viviano, C.E., 2013. A hematite-bearing layer in gale crater, mars: Mapping and implications for past aqueous conditions. Geology 41, 1103–1106. https://doi.org/10.1130/G34613.1.

Franz, H.B., King, P.L., Gaillard, F., 2019. Sulfur on mars from the atmosphere to the core. In: Filiberto, J., Schewenzer, S.P. (Eds.), Volatiles in the Martian Crust. Elsevier, pp. 119–183. https://doi.org/10.1016/B978-0-12-804191-8.00006-4.

Freeman, John J., Alian Wang, J.J., Kuebler, K.E., Haskin, L.A., 2008. Characterization of natural feldspar by Raman spectroscopy for future planetary exploration. Can. Mineral. 46, 1477–1500. https://doi.org/10.3749/canmin.46.6.1477.

Garry, J.R.C., Loes ten Kate, I., Martins, Z., Nørnberg, P., Ehrenfreund, P., 2006. Analysis and survival of amino acids in Martian regolith analogs. Meteorit. Planet. Sci. 41, 391–405. https://doi.org/10.1111/j.1945-5100.2006.tb00470.x.

Geissler, P.E., Singer, R.B., Komatsu, G., Murchie, S., Mustard, J., 1993. An unusual spectral unit in west candor Chasma: evidence for aqueous or hydrothermal alteration in the martian canyons. Icarus 106, 380–391. https://doi.org/10.1006/ICAR.1993.1179.

Gellert, R., 2013. Mars Science Laboratory Alpha Particle X-Ray Spectrometer RDR Data V1.0. MSL-M-APXS-4/5-RDR-V1.0, NASA Planetary Data System.

Gellert, R., Rieder, R., Anderson, R.C., Bruckner, J., Clark, B.C., Dreibus, G., Economou, T., Klingelhöfer, G., Lugmair, G.W., Ming, D.W., Squyres, S.W., d'Uston, C., Wanke, H., Yen, A., Zipfel, J., 2004. Chemistry of rocks and soils in Gusev Crater from the alpha-particle x-ray spectrometer. Science 305, 829–832. https://doi.org/10.1126/science.1099913.

Gellert, R., Rieder, R., Brückner, J., Clark, B.C., Dreibus, G., Klingelhöfer, G., Lugmair, G., Ming, D.W., Wänke, H., Yen, A., Zipfel, J., Squyres, S.W., 2006. Alpha particle X-ray spectrometer (APXS): results from Gusev Crater and calibration report. J. Geophys. Res. E Planets 111. https://doi.org/10.1029/2005JE002555.

Gellert, R., Berger, J.A., Boyd, N., Brunet, C., Campbell, J.L., Curry, M., Elliott, B., Fulford, P., Grotzinger, J., Hipkin, V., Hurowitz, J., King, P.L., Leshin, L., Limonadi, D., Pavri, B., Pradler, I., Marchand, G., Perrett, G.M., Scodary, A., Simmonds, J.J., Spray, J., Squyres, S.W., Thompson, L., Vanbommel, S., Yen, A.S., 2013. Initial MSL APXS Activities and Observations at Gale Crater, Mars, Lunar and Planetary Science Conference. Abstract# 1432.

Glotch, T.D., Bandfield, J.L., Tornabene, L.L., Jensen, H.B., Seelos, F.P., 2010. Distribution and formation of chlorides and phyllosilicates in Terra Sirenum, mars. Geophys. Res. Lett. 37, 1–5. https://doi.org/10.1029/2010GL044557.

Golombek, M.P., Cook, R.A., Economou, T., Folkner, W.M., Haldemann, A.F., Kallemeyn, P.H., Knudsen, J.M., Manning, R.M., Moore, H.J., Parker, T.J., Rieder, R., Schofield, J.T., Smith, P.H., Vaughan, R.M., 1997. Overview of the Mars Pathfinder mission and assessment of landing site predictions. Science 278, 1743–1748. https://doi.org/10.1126/SCIENCE.278.5344.1743.

Govindaraju, K., 1994. 1994 compilation of working values and sample description for 383 geostandards. Geostand. Newsl. 18, 1–158.

Gross, F.B., Grek, S.B., Calle, C.I., Lee, R.U., 2001. JSC Mars-1 Martian Regolith simulant particle charging experiments in a low pressure environment. J. Electrost. 53, 257–266. https://doi.org/10.1016/S0304-3886(01)00152-8.

Grotzinger, J.P., Sumner, D.Y., Kah, L.C., Stack, K., Gupta, S., Edgar, L., Rubin, D., Lewis, K., 2014. A habitable fluvio-lacustrine environment at yellowknife Bay, Gale crater, mars. Science 343, 1–18. https://doi.org/10.1126/science.1242777.

Hamilton, V.E., Christensen, P.R., McSween, H.Y., Bandfield, J.L., 2010. Searching for the source regions of martian meteorites using MGS TES: Integrating martian meteorites into the global distribution of igneous materials on Mars. Meteorit. Planet. Sci. 38, 871–885. https://doi.org/10.1111/j.1945-5100.2003.tb00284.x.

Huang, E., Chen, C.H., Huang, T., Lin, E.H., Xu, J.A., 2000. Raman spectroscopic characteristics of Mg-Fe-Ca pyroxenes. Am. Mineral. 85, 473–479. https://doi.org/10.2138/am-2000-0408.

Hudson, T.L., Aharonson, O., Schorghofer, N., Farmer, C.B., Hecht, M.H., Bridges, N.T., 2007. Water vapor diffusion in Mars subsurface environments. J. Geophys. Res. E Planets 112, 1–27. https://doi.org/10.1029/2006JE002815.

Hynek, B.M., 2002. Geologic setting and origin of Terra Meridiani hematite deposit on Mars. J. Geophys. Res. 107, 5088. https://doi.org/10.1029/2002JE001891.

Imai, N., Terashim, a S., Itoh, S., Ando, A., 1995. 1994 compilation of analytical data for minor and trace elements in seventeen GSJ geochemical reference samples, "Igneous rock series": Geostand. Newsl. 19, 135–213.

Imai, N., Terashima, S., Itoh, S., Ando, A., 1996. 1996 compilation of analytical data on nine GSJ geochemical reference samples, "Sedimentary rock series". Geostand. Newsl. 20, 165–216.

Imai, N., Terashima, S., Itoh, S., Ando, A., 1999. 1998 compilation of analytical data for five GSL geochemical reference samples, the "Instrumental analysis series". Geostand. Newsl. 23, 223–250.

Klingelhöfer, G., Morris, R.V., Bernhardt, B., Schröder, C., Rodionov, D.S., de Souza Jr., P.A., Yen, A., Gellert, R., Evlanov, E.N., Zubkov, B., Foh, J., Bonnes, U., Kankeleit, E., Gütlich, P., Ming, D.W., Renz, F., Wdowiak, T., Squyres, S.W., Arvidson, R.E., 2004. Jarosite and hematite at Meridiani Planum from opportunity ' s Mössbauer spectrometer. Science 306, 1740–1745. https://doi.org/10.1126/science.1104653.

Kral, T.A., Bekkum, C.R., McKay, C.P., 2004. Growth of methanogens on a mars soil simulant. Orig. Life Evol. Biosph. 34, 615–626. https://doi.org/10.1023/B:ORIG.0000043129.68196.5f.

Kuebler, K.E., Jolliff, B.L., Wang, A., Haskin, L.A., 2006. Extracting olivine (Fo-Fa) compositions from Raman spectral peak positions. Geochem. Cosmochim. Acta 70, 6201–6222. https://doi.org/10.1016/j.gca.2006.07.035.

Lafuente, B., Downs, R.T., Yang, H., Stone, N., 2015. The Power of Databases: the RRUFF Project, Highlights Mineralogical Crystallography. W. De Gruyter, Berlin, pp. 1–30.

Lane, M.D., Bishop, J.L., Dyar, M.D., King, P.L., Parente, M., Hyde, B.C., 2008. Mineralogy of the Paso Robles soils on mars. Am. Mineral. 93, 728–739. https://doi.org/10.2138/am.2008.2757.

Lōpez, A., Frost, R.L., 2015. Raman spectroscopy of pyrite in marble from Chillagoe, Queensland. J. Raman Spectrosc. 46, 1033–1036. https://doi.org/10.1002/jrs.4699.

Martín-Torres, F.J., Zorzano, M.-P., Valentín-Serrano, P., Harri, A.-M., Genzer, M., Kemppinen, O., Rivera-Valentin, E.G., Jun, I., Wray, J., Bo Madsen, M., Goetz, W., McEwen, A.S., Hardgrove, C., Renno, N., Chevrier, V.F., Mischna, M., Navarro-González, R., Martínez-Frías, J., Conrad, P., McConnochie, T., Cockell, C., Berger, G., R. Vasavada, A., Sumner, D., Vaniman, D., 2015. Transient liquid water and water activity at Gale crater on Mars. Nat. Geosci. 8, 357–361. https://doi.org/10.1038/ngeo2412.

McSween, H.Y., Arvidson, R.E., Bell, J.F., Blaney, D., Cabrol, N.A., Christensen, P.R., Clark, B.C., Crisp, J.A., Crumpler, L.S., Des Marias, D.J., Farmer, J.D., Gellert, R.,

Ghosh, A., Gorevan, S., Graff, T., Grant, J., Haskin, L.A., Herkenhoff, K.E., Johnson, J.R., Jolliff, B.L., Klingelhoefer, G., Knudson, A.T., McLennan, S., Milam, K.A., Moersch, J.E., Morris, R.V., Rieder, R., Ruff, S.W., De Souza, P.A., Squyres, S.W., Wänke, H., Wang, A., Wyatt, M.B., Yen, A., Zipfel, J., 2004. Basaltic rocks analyzed by the Spirit rover in Gusev crater. Science 305, 842–845. https://doi.org/10.1126/science.3050842.

McSween, H.Y., Taylor, G.J., Wyatt, M.B., 2009. Elemental composition of the martian crust. Science 324, 736–739. https://doi.org/10.1126/science.1165871.

Moore, H.J., Jakosky, B.M., 1989. Viking landing sites, remote-sensing observations, and physical properties of Martian surface materials. Icarus 81, 164–184. https://doi.org/10.1016/0019-1035(89)90132-2.

Moore, H.J., Hutton, R.E., Clow, G.D., Spitzer, C.R., 1987. Physical properties of the surface materials at the Viking landing sites on mars. U. S. Geol. Surv. Prof. Pap. 1389, 1–222.

Moors, H.J., De Craen, M., 2018. A physico-chemical and geo-microbiological study of ten different lakes located in the Danakil depression. In: European Planetary Science Conference. Absrtact# EPSC2018–1152–1. https://doi.org/10.1029/2002JE001852.

Moroz, L.V., Basilevsky, A.T., Hiroi, T., Rout, S.S., Baither, D., van der Bogert, C.H., Yakovlev, O.I., Fisenko, A.V., Semjonova, L.F., Rusakov, V.S., Khramov, D.A., Zinovieva, N.G., Arnold, G., Pieters, C.M., 2009. Spectral properties of simulated impact glasses produced from martian soil analogue JSC Mars-1. Icarus 202, 336–353. https://doi.org/10.1016/j.icarus.2009.02.007.

Morris, R.V., Klingelhöfer, G., Bernhardt, B., Schröder, C., Rodionov, D.S., de Souza Jr., P.A., Yen, A., Gellert, R., Evlanov, E.N., Foh, J., Kankeleit, E., Gütlich, P., Ming, D.W., Renz, F., Wdowiak, T., Squyres, S.W., Arvidson, R.E., 2004. Mineralogy at Gusev Crater from the Mössbauer spectrometer on the Spirit rover. Science 305, 833–836. https://doi.org/10.1126/science.1100020.

Morris, R.V., Klingelhöfer, G., Schröder, C., Rodionov, D.S., Yen, A., Ming, D.W., de Souza Jr., P.A., Fleischer, I., Wdowiak, T., Gellert, R., Bernhardt, B., Evlanov, E.N., Zubkov, B., Foh, J., Bonnes, U., Kankeleit, E., Gütlich, P., Renz, F., Squyres, S.W., Arvidson, R.E., 2006a. Mössbauer mineralogy of rock, soil, and dust at Gusev crater, Mars: Spirit's journey through weakly altered olivine basalt on the plains and pervasively altered basalt in the Columbia Hills. J. Geophys. Res. 111, E02S13. https://doi.org/10.1029/2005JE002584.

Morris, R.V., Klingelhöfer, G., Schröder, C., Rodionov, D.S., Yen, A., Ming, D.W., de Souza Jr., P.A., Wdowiak, T., Fleischer, I., Gellert, R., Bernhardt, B., Bonnes, U., Cohen, B.A., Evlanov, E.N., Foh, J., Gütlich, P., Kankeleit, E., McCoy, T., Mittlefehldt, D.W., Renz, F., Schmidt, M.E., Zubkov, B., Squyres, S.W., Arvidson, R.E., 2006b. Mössbauer mineralogy of rock, soil, and dust at Meridiani Planum, Mars: opportunity's journey across sulfate-rich outcrop, basaltic sand and dust, and hematite lag deposits. J. Geophys. Res. 111, E12S15. https://doi.org/10.1029/2006JE002791.

Morris, R.V., Klingelhöfer, G., Schröder, C., Fleischer, I., Ming, D.W., Yen, A.S., Gellert, R., Arvidson, R.E., Rodionov, D.S., Crumpler, L.S., Clark, B.C., Cohen, B.A., McCoy, T.J., Mittlefehldt, D.W., Schmidt, M.E., de Souza Jr., P.A., Squyres, S.W., 2008. Iron mineralogy and aqueous alteration from husband hill through home plate at Gusev Crater, mars: results from the Mössbauer instrument on the Spirit mars exploration rover. J. Geophys. Res. 113, E12S42. https://doi.org/10.1029/2008JE003201.

Morris, R.V., Vaniman, D.T., Blake, D.F., Gellert, R., Chipera, S.J., Rampe, E.B., Ming, D.W., Morrison, S.M., Downs, R.T., Treiman, A.H., Yen, A.S., Grotzinger, J.P., Achilles, C.N., Bristow, T.F., Crisp, J.A., Des Marais, D.J., Farmer, J.D., Fendrich, K.V., Frydenvang, J., Graff, T.G., Morookian, J.-M., Stolper, E.M., Schwenzer, S.P., 2016. Silicic volcanism on Mars evidenced by tridymite in high-SiO2 sedimentary rock at Gale crater. Proc. Natl. Acad. Sci. U.S.A. 113, 7071–7076. https://doi.org/10.1073/pnas.1607098113.

Mouri, T., Enami, M., 2008. Raman spectroscopic study of olivine-group minerals. J. Mineral. Petrol. Sci. 103, 100–104. https://doi.org/10.2465/jmps.071015.

Murchie, S.L., Mustard, J.F., Ehlmann, B.L., Milliken, R.E., Bishop, J.L., McKeown, N.K., Noe Dobrea, E.Z., Seelos, F.P., Buczkowski, D.L., Wiseman, S.M., Arvidson, R.E., Wray, J.J., Swayze, G., Clark, R.N., Des Marais, D.J., McEwen, A.S., Bibring, J.P., 2009. A synthesis of Martian aqueous mineralogy after 1 Mars year of observations from the Mars Reconnaissance Orbiter. J. Geophys. Res. E Planets 114, 1–30. https://doi.org/10.1029/2009JE003342.

Mustard, J.F., Poulet, F., Gendrin, A., Bibring, J.-P., Langevin, Y., Gondet, B., Mangold, N., Bellucci, G., Altieri, F., 2005. Olivine and pyroxene diversity in the crust of Mars. Science 307, 1594–1597. https://doi.org/10.1126/science.1109098.

Mustard, J.F., Murchie, S.L., Pelkey, S.M., Ehlmann, B.L., Milliken, R.E., Grant, J.A., Bibring, J.-P., Poulet, F., Bishop, J., Dobrea, E.N., Roach, L., Seelos, F., Arvidson, R.E., Wiseman, S., Green, R., Hash, C., Humm, D., Malaret, E., McGovern, J.A., Seelos, K., Clancy, T., Clark, R., Des Marais, D., Izenberg, N., Knudson, A., Langevin, Y., Martin, T., McGuire, P., Morris, R., Robinson, M., Roush, T., Smith, M., Swayze, G., Taylor, H., Titus, T., Wolff, M., 2008. Hydrated silicate minerals on mars observed by the mars reconnaissance orbiter CRISM instrument. Nature 454, 305–309. https://doi.org/10.1038/nature07097.

Nachon, M., Clegg, S.M., Mangold, N., Schröder, S., Kah, L.C., Dromart, G., Ollila, A., Johnson, J.R., Oehler, D.Z., Bridges, J.C., Le Mouélic, S., Forni, O., Wiens, R.C., Anderson, R.B., Blaney, D.L., Bell, J.F., Clark, B., Cousin, A., Dyar, M.D., Ehlmann, B., Fabre, C., Gasnault, O., Grotzinger, J., Lasue, J., Lewin, E., Léveillé, R., McLennan, S., Maurice, S., Meslin, P.Y., Rapin, W., Rice, M., Squyres, S.W., Stack, D.Y., Sumner, D.Y., Vaniman, D., Wellington, D., 2014. Calcium sulfate veins characterized by ChemCam/Curiosity at Gale crater, mars. J. Geophys. Res. E Planets 119, 1991–2016. https://doi.org/10.1002/2013JE004588.

Nixon, S.L., Cousins, C.R., Cockell, C.S., 2013. Plausible microbial metabolisms on Mars. Astron. Geophys. 54, 13–16. https://doi.org/10.1093/astrogeo/ats034.

Nørnberg, P., Schwertmann, U., Stanjek, H., Andersen, T., Gunnlaugsson, H.P., 2004. Mineralogy of a burned soil compared with four anomalously red Quaternary

deposits in Denmark. Clay Miner. 39, 85–98. https://doi.org/10.1180/0009855 043910122.

Nørnberg, P., Gunnlaugsson, H.P., Merrison, J.P., Vendelboe, A.L., 2009. Salten Skov I: a Martian magnetic dust analogue. Planet. Space Sci. 57, 628–631. https://doi.org/10.1016/j.pss.2008.08.017.

Olsson-Francis, K., Pearson, V.K., Steer, E.D., Schwenzer, S.P., 2017. Determination of geochemical bio-Signatures in mars-like basaltic environments. Front. Microbiol. 8, 1–17. https://doi.org/10.3389/fmicb.2017.01668.

Pacelli, C., Selbmann, L., Zucconi, L., De Vera, J.P., Rabbow, E., Horneck, G., de la Torre, R., Onofri, S., 2017. BIOMEX experiment: ultrastructural alterations, Molecular damage and survival of the fungus cryomyces antarcticus after the experiment Verification tests. Orig. Life Evol. Biosph. 47, 187–202. https://doi.org/10.1007/s11084-016-9485-2.

Peters, G.H., Abbey, W., Bearman, G.H., Mungas, G.S., Smith, J.A., Anderson, R.C., Douglas, S., Beegle, L.W., 2008. Mojave Mars simulant-Characterization of a new geologic Mars analog. Icarus 197, 470–479. https://doi.org/10.1016/j.icarus.2008.05.004.

Phebus, B.D., Johnson, A.V., Mar, B., Stone, B.M., Colaprete, A., Iraci, L.T., 2011. Water ice nucleation characteristics of JSC Mars-1 regolith simulant under simulated Martian atmospheric conditions. J. Geophys. Res. E Planets 116, 1–8. https://doi.org/10.1029/2010JE003699.

Poulet, F., Gomez, C., Bibring, J.P., Langevin, Y., Pinet, P., Belluci, G., Mustard, J., 2007. Martian surface mineralogy from Observatoire pour la Minéralogie, l'Eau, les Glaces et l'Activité on board the Mars Express spacecraft (OMEGA/MEx): global mineral maps. J. Geophys. Res. E Planets 112, 1–15. https://doi.org/10.1029/2006JE002840.

Powers, M.C., 1953. A new roundness Scale for sedimentary particles. SEPM J. Sediment. Res. 23, 117–119. https://doi.org/10.1306/D4269567-2B26-11D7-8648000102C1 865D.

Rancourt, D.G., Ping, J.Y., 1991. Voigt-based methods for arbitrary-shape static hyperfine parameter distributions in Mössbauer spectroscopy. Nucl. Instrum. Methods Phys. Res. 58, 85–97. https://doi.org/10.1016/0168-583X(91)95681-3.

Richter, L., Coste, P., Gromov, V., Kochan, H., Nadalini, R., Ng, T., Pinna, S., Richter, H.-E., Yung, K., 2002. Development and testing of subsurface sampling devices for the Beagle 2 lander. Planet. Space Sci. 50, 903–913. https://doi.org/10.1016/S0032-0633(02)00066-1.

Rieder, R., Gellert, R., Anderson, R.C., Bruckner, J., Clark, B.C., Dreibus, G., Economou, T., Klingelhofer, G., Lugmair, G.W., Ming, D.W., Squyres, S.W., D'Uston, C., Wanke, H., Yen, A., Zipfel, J., 2004. Chemistry of rocks and soils at Meridiani Planum from the alpha particle X-ray spectrometer. Science 305, 1746–1749. https://doi.org/10.1126/science.1099913.

Rull, F., Maurice, S., Hutchinson, I., Moral, A., Perez, C., Diaz, C., Colombo, M., Belenguer, T., Lopez-Reyes, G., Sansano, A., Forni, O., Parot, Y., Striebig, N., Woodward, S., Howe, C., Tarcea, N., Rodriguez, P., Seoane, L., Santiago, A., Rodriguez-Prieto, J.A., Medina, J.S., Gallego, P., Canchal, R., Santamaría, P., Ramos, G., Vago, J.L., 2017. The Raman laser spectrometer for the ExoMars rover mission to mars. Astrobiology 17, 627–654. https://doi.org/10.1089/ast.2016.1567.

Schirmack, J., Alawi, M., Wagner, D., 2015. Influence of Martian regolith analogs on the activity and growth of methanogenic archaea, with special regard to long-term desiccation. Front. Microbiol. 6, 1–12. https://doi.org/10.3389/fmicb.2015.00210.

Schmidt, M.E., Campbell, J.L., Gellert, R., Perrett, G.M., Treiman, A.H., Blaney, D.L., Olilla, A., Calef, F.J., Edgar, L., Elliott, B.E., Grotzinger, J., Hurowitz, J., King, P.L., Minitti, M.E., Sautter, V., Stack, K., Berger, J.A., Bridges, J.C., Ehlmann, B.L., Forni, O., Leshin, L.A., Lewis, K.W., McLennan, S.M., Ming, D.W., Newsom, H., Pradler, I., Squyres, S.W., Stolper, E.M., Thompson, L., VanBommel, S., Wiens, R.C., 2014. Geochemical diversity in first rocks examined by the Curiosity Rover in Gale Crater: evidence for and significance of an alkali and volatile-rich igneous source. J. Geophys. Res. Planets 119, 64–81. https://doi.org/10.1002/2013JE004481.

Schröder, C., Köhler, I., Muller, F.L.L., Chumakov, A.I., Kupenko, I., Rüffer, Rudolf, Kappler, A., 2016. The biogeochemical iron cycle and astrobiology. Hyperfine Interact. 237, 85. https://doi.org/10.1007/s10751-016-1289-2.

Schuerger, A.C., Golden, D.C., Ming, D.W., 2012. Biotoxicity of Mars soils: 1. Dry deposition of analog soils on microbial colonies and survival under Martian conditions. Planet. Space Sci. 72, 91–101. https://doi.org/10.1016/j.pss.2012.07.026.

Schwenzer, S.P., Bridges, J.C., Wiens, R.C., Conrad, P.G., Kelley, S.P., Leveille, R., Mangold, N., Martín-Torres, J., McAdam, A., Newsom, H., Zorzano, M.P., Rapin, W., Spray, J., Treiman, A.H., Westall, F., Fairén, A.G., Meslin, P.Y., 2016. Fluids during diagenesis and sulfate vein formation in sediments at Gale crater, Mars. Meteorit. Planet. Sci. 51, 2175–2202. https://doi.org/10.1111/maps.12668.

Schwenzer, S.P., Bridges, J.C., A, M.M., Hicks, L.J., Ott, U., Filiberto, J., C, C., H, S., Treiman, A.H., Kelley, S.P., Moore, J.M., D, S., Bullock, M.A., 2017. Diagenesis on mars: Insights into noble gas Pathways and newly formed mineral assemblages from long term experiments. In: Lunar and Planetary Science Conference. Abstract# 1344. https://doi.org/10.1002/2014JE.

Scott, G.P., Saaj, C.M., 2009. Measuring and Simulating the Effect of Variations in Soil Properties on Microrover Trafficability. American Institute of Aeronautics and Astronautics, Pasadena, pp. 1–10.

Scott, G.P., Saaj, C.M., 2012. The development of a soil trafficability model for legged vehicles on granular soils. J. Terramechanics 49, 133–146. https://doi.org/10.1016/J.JTERRA.2011.12.002.

Scott, A.N., Oze, C., Tang, Y., O'Loughlin, A., 2017. Development of a Martian regolith simulant for in-situ resource utilization testing. Acta Astronaut. 131, 45–49. https://doi.org/10.1016/j.actaastro.2016.11.024.

Seiferlin, K., Ehrenfreund, P., Garry, J., Gunderson, K., Hütter, E., Kargl, G., Maturilli, A., Merrison, J.P., 2008. Simulating Martian regolith in the laboratory. Planet. Space Sci. 56, 2009–2025. https://doi.org/10.1016/j.pss.2008.09.017.

Shorthill, R.W., Moore II, H.,J., Scott, R.F., Hutton, R.E., Liebes Jr., S., Spitzer, C.R., 1976. The " soil " of mars (Viking 1). Science 194, 91–97.

Smith, C.L., Manick, K., Duvet, L., Schroeven-Deceuninck, H., 2017. STARTING A European Space Agency Sample Analogue Collection (ESA²C) and Curation Facility for Exploration Missions, Lunar and Planetary Science Conference. Abstract# 1218.

Smith, C.L., Gill, S., Manick, K., Miller, C.G., Jones, C., Rumsey, M.S., Duvet, L., 2018a. The European Space Agency Exploration Sample Analogue Collection (ESA²C) and Curation Facility-Present and Future. Abstract# Lunar and Planetary Science Conference2, p. 1623.

Smith, C., Rumsey, M., Jones, C., Miller, G., Manick, K., Gill, S., Duvet, L., Vrublevskis, J., Berthoud, L., 2018b. European Space Agency: exploration sample analogue collection and curation facility. http://www.nhm.ac.uk/our-science/our-work/origins-evolu tion-and-futures/esa-exploration-sample-analogue-collection-curation-facility.html, 12.12.18.

Soderblom, L.A., Anderson, R.C., Arvidson, R.E., Bell, J.F., Cabrol, N.A., Calvin, W., Christensen, P.R., Clark, B.C., Economou, T., Ehlmann, B.L., Farrand, W.H., Fike, D., Gellert, R., Glotch, T.D., Golombek, M.P., Greeley, R., Grotzinger, J.P., Herkenhoff, K.E., Jerolmack, D.J., Johnson, J.R., Jolliff, B., Klingelhöfer, C., Knoll, A.H., Learner, Z.A., Li, R., Malin, M.C., McLennan, S.M., McSween, H.Y., Ming, D.W., Morris, R.V., Rice, J.W., Richter, L., Rieder, R., Rodionov, D., Schröder, C., Seelos IV, F.P., Soderblom, J.M., Squyres, S.W., Sullivan, R., Watters, W.A., Weitz, C.M., Wyatt, M.B., Yen, A., Zipfel, J., 2004. Soils of eagle crater and Meridiani Planum at the opportunity Rover landing site. Science 306, 1723–1726. https://doi.org/10.1126/science.1105127.

Squyres, S.W., Arvidson, R.E., Bell III, J.F., Calef III, F., Clark, B.C., Cohen, B.A., Crumpler, L.A., de Souza Jr., P.A., Farrand, W.H., Gellert, R., Grant, J., Herkenhoff, K.E., Hurowitz, J.A., Johnson, J.R., Jolliff, B.L., Knoll, A.H., Li, R., McLennan, S.M., Ming, D.W., Mittlefehldt, D.W., Parker, T.J., Paulsen, G., Rice, M.S., Ruff, S.W., Schröder, C., Yen, A.S., Zacny, K., 2012. Ancient impact and aqueous processes at endeavour crater, mars. Science 336, 570–576. https://doi.org/10.1126/science.1220476.

Stevens, A.H., Steer, E., McDonald, A., Amador, E.S., Cockell, C.S., 2018. Y-mars: an astrobiological analogue of martian mudstone. Earth Sp. Sci. 5, 163–174. https://doi.org/10.1002/2017EA000318.

Toulmin III, P., Baird, A.K., Clark, B.C., Keil, K., Rose Jr., H.J., Christian, R.P., Evans, P.H., Kelliher, W.C., 1977. Geochemical and mineralogical interpretation of the Viking Inorganic chemical results. J. Geophys. Res. 82, 4625–4634. https://doi.org/10.1029/JS082i028p04625.

Uroz, S., Calvaruso, C., Turpault, M.P., Frey-Klett, P., 2009. Mineral weathering by bacteria: ecology, actors and mechanisms. Trends Microbiol. 17, 378–387. https://doi.org/10.1016/j.tim.2009.05.004.

Van den Bogaard, P., Schmincke, H.U., 1990. The development history of the Middle Rhine area and the eruption history of the East Eifel volcanic field. In: Rhine History between Mosel and Maas, vol. 1. Deuqua Leader, pp. 166–190.

Vaniman, D.T., Bish, D.L., Ming, D.W., Bristow, T.F., Morris, R.V., Blake, D.F., 2014. Mineralogy of a mudstone at yellowknife Bay, Gale crater, mars. Science 343, 1–9. https://doi.org/10.1126/science.1243480.

Wang, A., Haskin, L.A., Squyres, S.W., Jolliff, B.L., Crumpler, L., Gellert, R., Schröder, C., Herkenhoff, K., Hurowitz, J., Tosca, N.J., Farrand, W.H., Anderson, R., Knudson, A.T., 2006. Sulfate deposition in subsurface regolith in Gusev crater, Mars. J. Geophys. Res. E Planets 111, 1–19. https://doi.org/10.1029/2005JE002513.

Wänke, H., Brückner, J., Dreibus, G., Rieder, R., Ryabchikov, I., 2001. Chemical composition of rocks and soils at the Pathfinder site. Space Sci. Rev. 96, 317–330. https://doi.org/10.1023/A:1011961725645.

Weitz, C.M., Anderson, R.C., Bell, J.F., Farrand, W.H., Herkenhoff, K.E., Johnson, J.R., Jolliff, B.L., Morris, R.V., Squyres, S.W., Sullivan, R.J., 2006. Soil grain analyses at Meridiani Planum, mars. J. Geophys. Res. E Planets 111, 1–26. https://doi.org/10.1029/2005JE002541.

Weitz, C.M., Lane, M.D., Staid, M., Dobrea, E.N., 2008. Gray hematite distribution and formation in Ophir and Candor chasmata. J. Geophys. Res. E Planets 113, 1–30. https://doi.org/10.1029/2007JE002930.

Weitz, C.M., Sullivan, R.J., Lapotre, M.G.A., Rowland, S.K., Grant, J.A., Baker, M., Yingst, R.A., 2018. Sand grain sizes and shapes in eolian Bedforms at Gale crater, mars. Geophys. Res. Lett. 45, 9471–9479. https://doi.org/10.1029/2018GL078972.

Wray, J.J., Noe Dobrea, E.Z., Arvidson, R.E., Wiseman, S.M., Squyres, S.W., McEwen, A.S., Mustard, J.F., Murchie, S.L., 2009. Phyllosilicates and sulfates at endeavour crater, Meridiani Planum, mars. Geophys. Res. Lett. 36, 1–5. https://doi.org/10.1029/2009GL040734.

Wu, L., Jacobson, A.D., Chen, H.-C., Hausner, M., 2007. Characterization of elemental release during microbe–basalt interactions at T=28°C. Geochem. Cosmochim. Acta 71, 2224–2239. https://doi.org/10.1016/j.gca.2007.02.017.

Yen, A.S., Gellert, R., Schröder, C., Morris, R.V., Bell III, J.F., Knudson, A.T., Clark, B.C., Ming, D.W., Crisp, J.A., Arvidson, R.E., Blaney, D., Brückner, J., Christensen, P.R., Des Marais, D.J., de Souza Jr., P.A., Economou, T.E., Ghosh, A., Hahn, B.C., Herkenhoff, K.E., Haskin, L.A., Hurowitz, J.A., Jolliff, B.L., Johnson, J.R., Klingelhöfer, G., Madsen, M.B., McLennan, S.M., McSween, H.Y., Richter, L., Rieder, R., Rodionov, D., Soderblom, L., Squyres, S.W., Tosca, N.J., Wang, A., Wyatt, M., Zipfel, J., 2005. An integrated view of the chemistry and mineralogy of martian soils. Nature 436, 49–54. https://doi.org/10.1038/nature03637.

Yen, A.S., Morris, R.V., Clark, B.C., Gellert, R., Knudson, A.T., Squyres, S., Mittlefehldt, D.W., Ming, D.W., Arvidson, R., McCoy, T., Schmidt, M., Hurowitz, J., Li, R., Johnson, J.R., 2008. Hydrothermal processes at Gusev Crater: an evaluation of Paso Robles class soils. J. Geophys. Res. E Planets 113, 1–19. https://doi.org/10.1029/2007JE002978.

Zeng, X., Li, X., Wang, S., Li, S., Spring, N., Tang, H., Li, Y., Feng, J., 2015. JMSS-1: a new Martian soil simulant Planetary science. Earth Planets Space 67, 1–10. https://doi.org/10.1186/s40623-015-0248-5.